R-08-69

Review of possible correlations between in situ stress and PFL fracture transmissivity data at Forsmark

Derek Martin, University of Alberta

Sven Follin, SF GeoLogic AB

November 2011

Svensk Kärnbränslehantering AB
Swedish Nuclear Fuel
and Waste Management Co

Box 250, SE-101 24 Stockholm
Phone +46 8 459 84 00

ISSN 1402-3091
SKB R-08-69

Review of possible correlations between in situ stress and PFL fracture transmissivity data at Forsmark

Derek Martin, University of Alberta

Sven Follin, SF GeoLogic AB

November 2011

Keywords: SKBdoc 1316711, Forsmark, Hydrogeology, Hydraulic tests, Difference flow logging, Transmissivity, Stress, Dilation, Slip, Scale.

Preface

The analyses presented in this report were completed in 2008, and the written report has been finalised in 2011. Despite the gap in time, the written report does not reflect any work beyond the effort of 2008. The significant results of the analyses were available to the site descriptive modelling at Forsmark, and were transferred to higher-level studies in time for groundwater flow modelling of the complete site investigation phase. Hence, we do not believe the results of this investigation affect or alter the conclusions of site assessment activities that support site selection or licensing.

November 2011

Sven Follin
SF GeoLogic AB

Abstract

In laboratory samples, the fracture transmissivity decreases significantly as the confining stress increases. While these experimental relationships are widely accepted and validated on laboratory samples, it is unknown if such relationships exist in situ or if these relationships can be scaled from the centimetre-scale laboratory tests to the metre-scale of in situ fractures. The purpose of this work is to assess the relationship between the structural-hydraulic data gathered in deep, cored boreholes at Forsmark and the in situ stress state acting on the these fractures. In conclusion, there does not appear to be sufficient evidence from these analyses to support the notion that the magnitude of the flow along the fractures at Forsmark is solely controlled by the in situ stress acting on the fracture. This should not be surprising because the majority of the fractures formed more than 1 billion years ago and the current in situ stress state has only been active for the past 12 million years. It is more likely that the transmissivity values are controlled by fracture roughness, open channels within the fracture, fracture stiffness and fracture infilling material.

Sammanfattning

I laboratorieförsök på bergprover som innehåller en spricka har man observerat att sprickans transmissivitet avtar då omgivande tryck ökas. Det är oklart om det observerade sambandet mellan spricktransmissivitet och tryck i laboratorieskala gäller även i verkligheten, dvs om man kan överföra samband som härleds för enskilda sprickor i centimeterskala till verkliga sprickor i meterskala. Syftet med föreliggande arbete är att studera sambandet mellan spricktransmissivitet och omgivande tryck i verkliga data hämtade från kilometerlånga borrhål i Forsmark. Sammanfattningsvis konstateras att de utförda analyserna inte bekräftar att transmissiviteten hos naturliga bergsprickor enbart kontrolleras av rådande spänningsfält. Resultatet är inte överraskande med tanke på att de flesta sprickorna är mer än 1 000 miljoner år gamla, medan det nuvarande spänningsfältet bara har varit aktivt under ca 12 miljoner år. Det är troligt att grundvattenflödet genom bergsprickorna även påverkas av andra faktorer, t ex sprickornas råhet samt förekomst av kanaler och bildandet av sprickmineral.

Contents

1	**Introduction**	9
1.1	Background	9
1.2	Scope and objectives	9
1.3	This report	9
2	**Bedrock hydrogeological model**	11
2.1	Hydrogeological data	11
2.2	Hydraulic characteristics of the deformation zones (HCD)	17
2.3	Hydraulic characteristics of the fracture domains (HRD)	19
3	**Primary data**	23
3.1	Fracture transmissivity	23
3.2	Fracture orientation	24
3.3	In situ stress	24
3.4	Assumptions	26
4	**In situ stress vs PFL fracture transmissivity**	27
4.1	Frequency of PFL fracture transmissivity data	27
4.2	Analysis of ALL_PFL	27
4.3	Analysis of FFM_PFL	27
4.4	Analysis of ZFM_PFL	27
5	**Influence of dilation and slip on fracture transmissivity**	39
5.1	Theory	39
5.2	PFL fracture transmissivity data in deformation zones	40
6	**Discussion**	47
7	**Conclusions**	51
8	**References**	53

1 Introduction

1.1 Background

In laboratory samples, the fracture transmissivity decreases significantly as the confining stress increases. As shown by Raven and Gale (1985) the relationships observed can be expressed as:

$$T = T_0 \sigma_n^{\alpha} \tag{1-1}$$

where T_0 is the transmissivity at a normal stress of 1 MPa and α is the negative slope of the relationship between log(T) versus log(σ_n)), i.e.:

$$\log T = \log T_0 + \alpha \log \sigma_n \tag{1-2}$$

According to Indraratna et al. (1999), when the confining stress exceeds 10 MPa, little or no decrease in transmissivity occurs, irrespective of the type of permeating medium, air or water. Indraratna et al. (1999) concluded that this confining stress of 10 MPa was required to bring the fracture closure to its residual aperture, beyond which confining stress had little effect.

1.2 Scope and objectives

While the experimental relationships, such as given in Equation 1-1, are widely accepted and validated on laboratory samples, it is unknown if such relationships exist in situ or if these relationships can be scaled from the centimetre-scale laboratory tests to the metre-scale of in situ fractures. The purpose of this work is to assess the relationship between the structural-hydraulic data gathered in deep, cored boreholes at Forsmark and the stress state acting on the rock at depth.

1.3 This report

Chapter 1 presents the background as well as the scope and objectives of the work reported here.

Chapter 2 summarises the bedrock hydrogeological model and the current understanding of the site.

Chapter 3 describes the primary data and assumptions used in the analyses.

Chapter 4 presents the results from stress-transmissivity analyses.

Chapter 5 discusses the role of dilation and slip on PFL fracture transmissivity.

Chapter 6 contains a discussion and Chapter 7 the conclusions based on the work reported here.

2 Bedrock hydrogeological model

2.1 Hydrogeological data

The north-western part of the candidate area was selected as the target area/volume for the complete site investigation work, see Figure 2-1. The bedrock hydrogeological model is summarised in Follin (2008) and presented in more detail in Follin et al. (2007a, b, 2008).

Table 2-1 lists the 25 cored boreholes shown in Figure 2-1. These are investigated with the Posiva Flow Log (PFL) method and the Pipe String System (PSS) method. The hydraulic data acquired from these tests are used to parameterise the deterministically defined deformation zones and the fracture networks contained in the rock mass volumes in between the deformation zones. In SKB's approach to hydraulic assessment, the former are referred to as Hydraulic Conductor Domains (HCD), whereas the latter are referred to as Hydraulic Rock mass Domains (HRD).

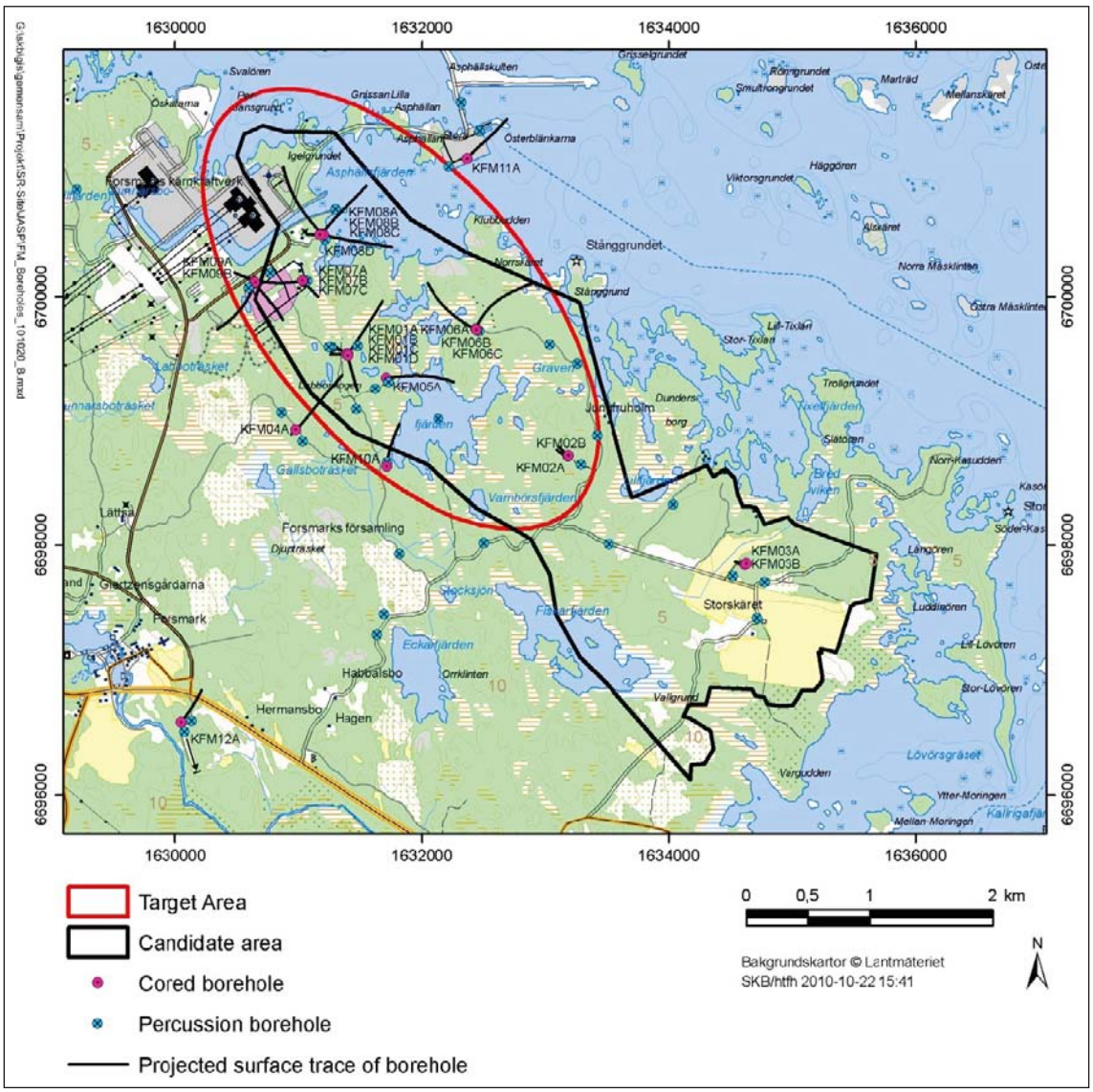

Figure 2-1. *Map showing the 25 core-drilled and the 38 percussion-drilled boreholes produced during the site investigation at Forsmark between years 2002–2007. The projection of the boreholes on the ground surface due to their inclination is also shown. The ellipse indicates the target area/volume. Modified after Figure A-1 in Follin (2008).*

Table 2-1. List of the cored boreholes at Forsmark tested with the PFL and PSS methods. Modified after Table B-4 in Follin et al. (2008).

Borehole	PFL	PSS	Bottom elevation of borehole (m)	Borehole	PFL	PSS	Bottom elevation of borehole (m)
KFM01A	X	X	–982	KFM07A	X		–819
KFM01B		X	–479	KFM07B		X	–238
KFM01C		X	–333	KFM07C	X		–494
KFM01D	X	X	–612	KFM08A	X	X	–759
KFM02A	X	X	–987	KFM08B		X	–166
KFM02B	X	X	–565	KFM08C	X		–781
KFM03A	X	X	–987	KFM08D	X		–751
KFM03B		X	–88	KFM09A		X	–621
KFM04A	X	X	–796	KFM09B		X	–472
KFM05A	X	X	–825	KFM10A	X	X	–338
KFM06A	X	X	–826	KFM11A	X	X	–716
KFM06B	X	X	–93	KFM12A		X	–511
KFM06C		X	–781				

The 38 percussion-drilled boreholes shown in Figure 2-1 are investigated by means of open hole pumping tests in combination with impeller flow logging (HTHB method). The hydraulic data acquired from these tests are used to parameterise the horizontal to sub-horizontal sheet joints that occur in the uppermost 150 m of the bedrock within the north-western part of the tectonic lens. This part of the flow model domain is called the shallow bedrock aquifer, see Follin (2008) for details.

Table 2-2 presents the terminology of brittle structures based on trace length and thickness.

The borderlines between the different structures are approximate. The three-dimensional block model contains 131 deterministically modelled deformation zones. These are referred to as ZFM plus an identification label. All but 39 deformation zones have trace lengths longer than one kilometre.

Figure 2-2 shows a 3D visualisation of the 131 deformation zones modelled deterministically in the hydrogeological SDM for Forsmark stage 2.2 (Follin et al. 2007b). The local model domain encompasses the target volume, hence investigated to a greater extent than the regional model domain. The bottom of the local model ends at the elevation –1,200 m, which means that it matches fairly well the maximum penetration depths of the deepest cored boreholes.

Table 2-3 shows a summary of the information presented above. We note in particular:

- 39 deformation zones have trace lengths shorter than one kilometre and 45 deformation zones have trace lengths longer than three kilometres.
- 59 of the 131 deformation zones contained by the 3D deformation zone model occur inside the local model domain solely, 43 major deformation zones occur outside the local model domain solely and 29 major deformation zones occur both inside and outside.

Table 2-2. Terminology and general description (length and width are approximate) of brittle structures. Modified after Table 4-1 in Andersson et al. (2000).

Terminology	Length	Width	Geometrical description
Regional	> 10 km	> 100 m	Deterministic
Local major	1 km–10 km	5 m–100 m	Deterministic (with scale-dependent description of uncertainty
Local minor	10 m–1 km	0.1–5 m	Stochastic (if possible, deterministic)
Fracture	< 10 m	< 0.1 m	Stochastic

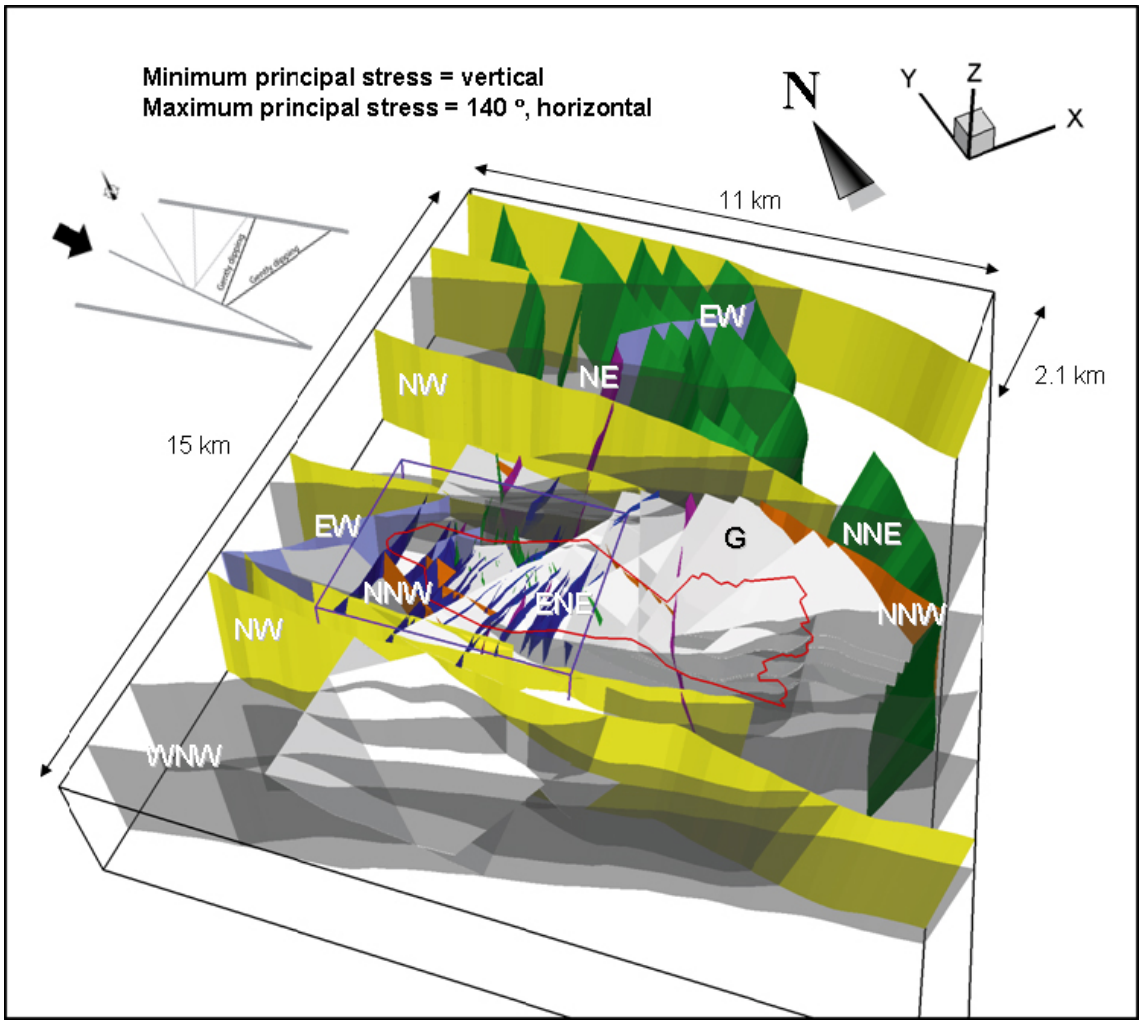

Figure 2-2. *3D visualisation of the regional model domain and the 131 deformation zones modelled deterministically for Forsmark stage 2.2 (Stephens et al. 2007). The steeply dipping deformation zones (107) are shaded in different colours and labelled with regard to their principle direction of strike. The gently dipping zones (24) are shaded in pale grey and denoted by a G. The border of the candidate area is shown in red and regional and local model domains in black and purple, respectively. The inset in the upper left corner of the figure shows the direction of the regional NW-SE oriented maximum horizontal stress.*

Table 2-3. Summary of trace length data (L) for the deterministically modelled deformation zones tabulated with regard to orientation. Note that ten of the 24 gently dipping deformation zones do not outcrop. The two numbers separated by a slash in the second and fifth columns show the number of major and minor deformations zones, respectively. All minor deformation zones are steeply dipping and shorter than 1 km. The colours shown in the table correspond to the colours used in Figure 2-2.

Orientation category	No. of DZ major/minor	No. of DZ L ≥ 3 km	No. of DZ 3 km > L ≥ 1 km	No. of DZ L < 1 km major/minor
G	24 / –	6	6	2 / –
WNW	23 / 1	15	7	1 / 1
NW	9 / –	9	0	0 / –
NNW	4 / 3	1	2	1 / 3
NNE	13 / 10	8	4	1 / 10
NE	4 / 6	2	1	1 / 6
ENE	24 / 7	2	17	5 / 7
EW	2 / 1	2	0	0 / 1
Total	103 / 28	45	37	11 / 28

Figure 2-3 shows three profile planes (cross-sections); one WNW-ESE cross-section along the central part of the candidate volume and two parallel WSW-ENE cross-sections in the eastern and central parts of the local model volume, respectively. (Profile plane (c) in Figure 2-3 is not shown in detail in Figure 2-3. It is located 1,255 m north-west of cross-section (b) in Figure 2-3 and parallel.)

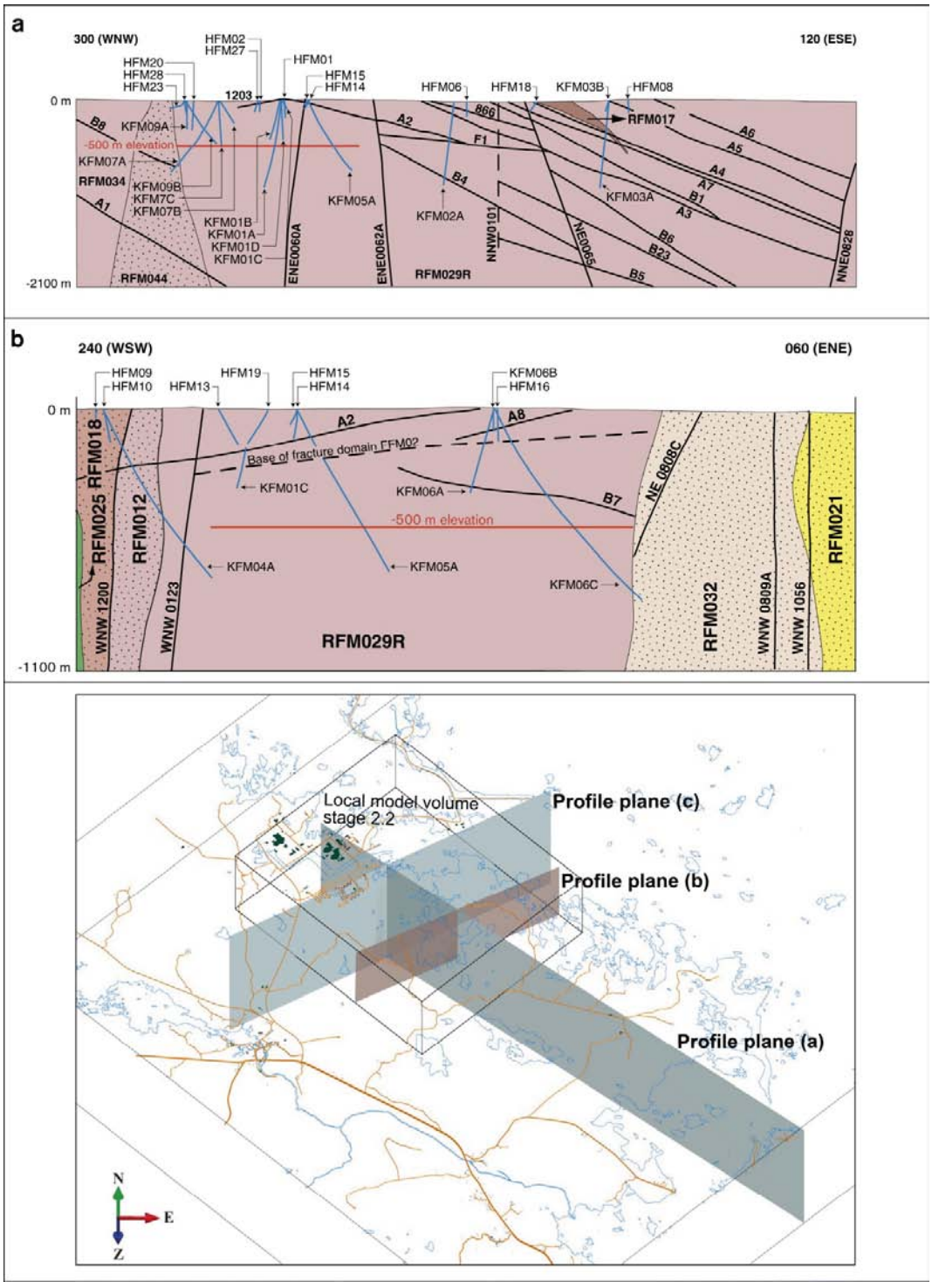

Figure 2-3. *Profile plane (a): A c. 7 km long WNW-ESE cross-section along the central part of the candidate volume. Profile plane (b) A c. 3 km long WSW-ENE cross-section along the south-eastern part of the local model volume. The important gently dipping deformation zones identified with reflection seismics are highlighted in these cross-sections. The bedrock above and below deformation zones A2 and F1 are referred to here as the hanging wall and the footwall, respectively. RFM029R is a regional rock domain. On a local scale RFM029R is split into the local rock domains RFM029 and RFM045.*

The WNW-ESE cross-section demonstrates the significant structural difference in the deformation zone pattern on both sides of the gently dipping and sub-horizontal deformation zones A2 and F1, respectively. The bedrock above these zones is here referred to as the *hanging wall* and the bedrock below as the *footwall*. The hanging wall bedrock contains a number of gently dipping deformation zones, many of which extend down to one kilometre depth, or more. In contrast, there are less gently dipping zones in the footwall bedrock. The difference in the deformation pattern between the hanging wall and the footwall is steered by, among other things, the older anisotropy at the site, with gently dipping ductile structures and rock contacts in the south-eastern part of the candidate volume and more steeply dipping structures and contacts in the north-western part, in different parts of a major, sheath fold structure (Stephens et al. 2007). It should be noted that the bedrock to the north-west of the steeply dipping deformation zone referred to as NE0065, both above and below zones A2 and F1, is intersected by a number of steeply dipping brittle deformation zones (fracture zones), many of which strike NNE and ENE. For purposes of simplicity, however, only the two zones that are included in the regional model are shown in Figure 2-3, i.e. ENE0060A and ENE0062A.

The fractured rock mass volumes between the deterministically modelled deformation zones are divided into six fracture domains, FFM01–FFM06 based on the fracture frequency of *all* fractures (Olofsson et al. 2007). The key fracture domains in the target area/volume aimed for a deep repository; FFM01 and FFM06, occur below fracture domain FFM02, see Figure 2-4 and Figure 2-5.

At Forsmark, the HRD geometries are identical to the geometries of the fracture domains. However, the six fracture domains are refined in the hydrogeological modelling based on the differences observed in the frequency of flowing fractures (conductive fracture frequency) versus depth, see Follin (2008) for details. The primary data used for this refinement come from the difference flow logging measurements carried out with the PFL method, see Follin et al. (2007a) for details. In summary, three of the six fracture domains are split into two sub-units each (FFM03FFM05) and two fracture domains are split into three sub-units each (FFM01 and FFM06). One fracture domain was left unchanged (FFM02).

Structural-hydraulic data from twelve cored boreholes (Follin et al. 2007a) are used in the detailed hydrogeological modelling of the target area/volume. The twelve boreholes are drilled at different locations and in different orientations in the rock mass volumes surrounding the repository. Figure 2-6 shows a view of the borehole locations with upper layers transparent.

Figure 2-7 shows examples of PFL data[1] from four cored boreholes, KFM01D, KFM06A–8A, located at drill sites 1, 6, 7 and 8, respectively. As can be seen in the plots, the bedrock has a high frequency of conductive fractures above –200 m, whereas below –400 m the frequency of conductive fractures decreases significantly. The decrease in PFL fracture transmissivity is not as significant as the decrease in frequency, although the highest PFL fracture transmissivity values are clearly observed above –200 m. These observations are commented in more detail in the text below. For the sake of clarity, it is noted that a casing is installed in the cored boreholes, which prohibits a detailed characterisation of the uppermost 100 m of bedrock with the PFL and PSS methods. Instead, the hydraulic characterisation of the uppermost bedrock is made with the HTHB method as described above. A detailed description of the three different test methods, PFL, PSS and HTHB, is found in Follin et al. (2007a).

[1] The flow rate at an intersecting flowing fracture is measured twice with the PFL method; first at natural head conditions and second with pumped head conditions. The difference in flow rate is divided by the difference in hydraulic head and the ratio defines the specific capacity at the fracture intercept. In SKB's database, Sicada, the specific capacity at an intersecting flowing fracture determined with the PFL method is called fracture transmissivity. More information on this matter is found in Chapter 3.

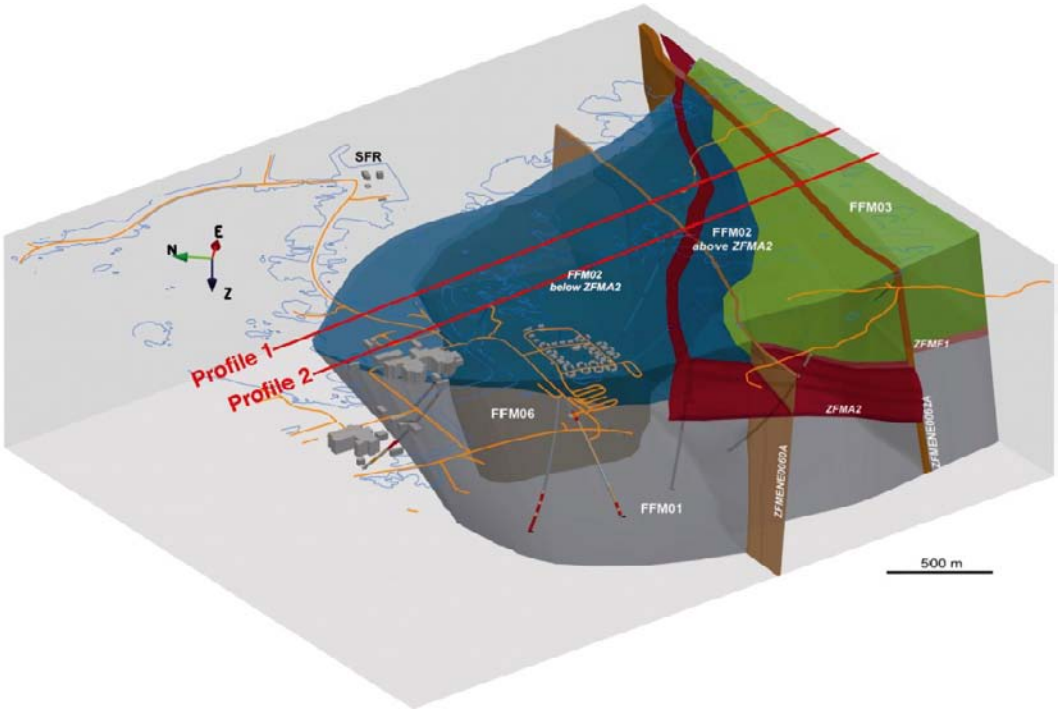

Figure 2-4. *Three-dimensional view to the East-North-East showing the relationship between deformation zone ZFMA2 (red) and fracture domain FFM01–03 and FFM06. Profile 1 and 2 are shown as cross-sections in Figure 2-5.*

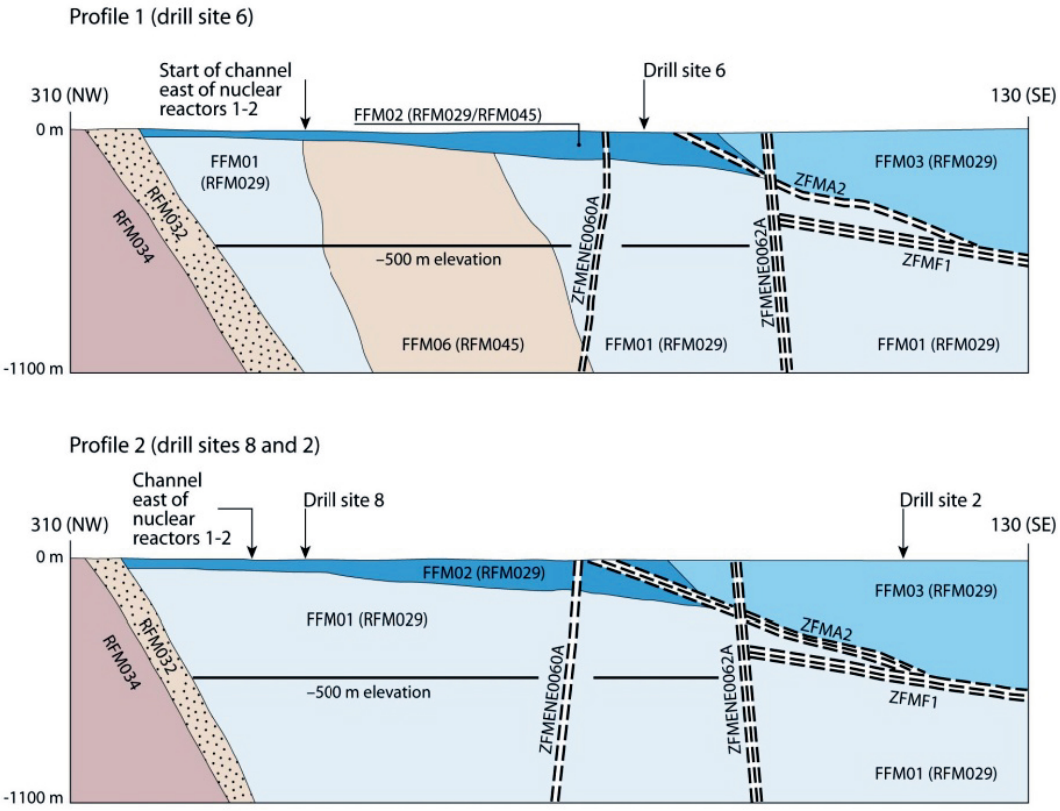

Figure 2-5. *Simplified profiles in a NW-SE direction that pass through drill sites 2 and 8 (lower profile) and drill site 6 (upper profile), cf. Figure 2-4 The key fracture domains FFM01, -02 and -06 occur in the footwall of zones ZFMA2 (gently dipping) and ZFMF1 (sub-horizontal). The major steeply dipping zones ZFMENE0060A and ZFMENE0062A are also included in these images.*

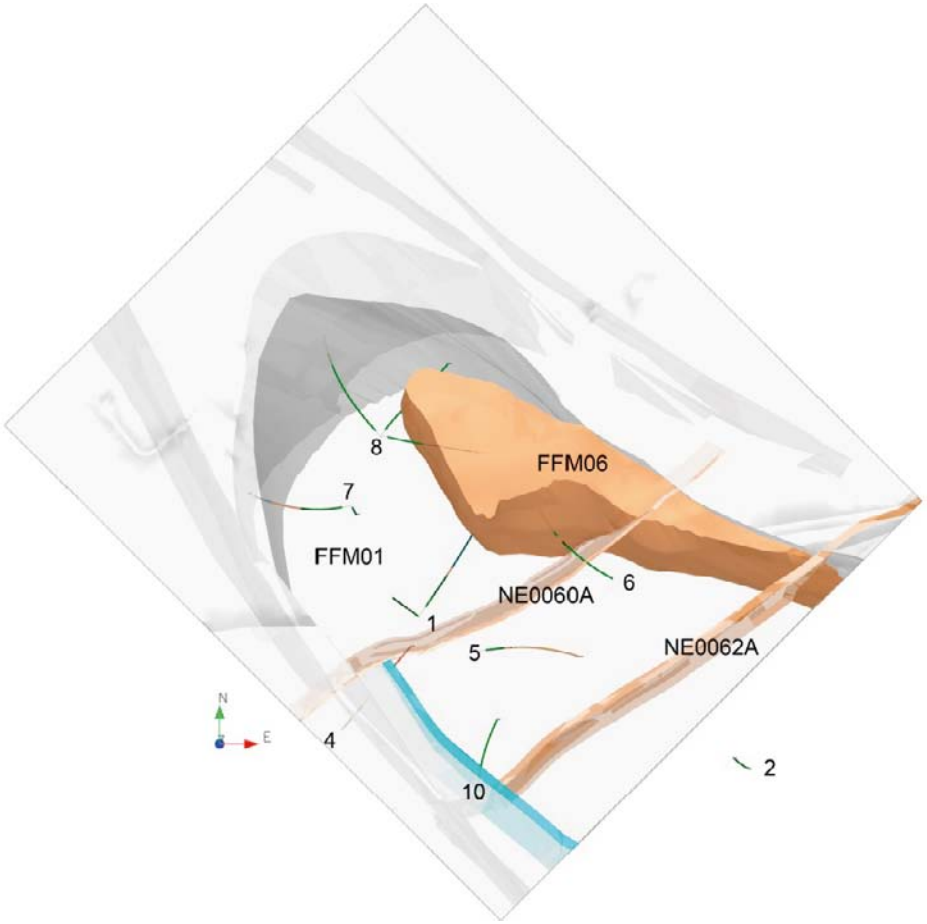

Figure 2-6. *View of the target area/volume with the regolith and FFM02 transparent showing the key fracture domains, FFM01 (transparent) and FFM06 (brownish). The lines represent cored boreholes and the labels represent drill site numbers (1, 2, 4–8, 10). NE0060A and NE0062A are two major deformation zones, see Figure 2-5.*

2.2 Hydraulic characteristics of the deformation zones (HCD)

The in-plane transmissivities of the deterministically modelled deformation zones are obtained by a summation of the PSS and PFL measurements from the intersection boreholes. That is, the summation of the PSS and PFL measurements is made between the upper and lower bounds of each deformation zone intercept. The results are shown in Figure 2-8, where the transmissivities are coloured with regard to the orientations of the zones. Here, G means gently dipping and the steeply dipping zones are denoted by their strike direction. The deformation zones with no measurable flow are assigned an arbitrary low transmissivity value of 1×10^{-10} m^2/s in order to make them visible on the log scale. The transmissivity data that are marked up by slightly larger squares with a white cross in the centre represent data that were acquired for verification purposes, see Follin et al. (2008).

As can be seen in the figure, there is a considerable lateral heterogeneity in the in-plane deformation zone transmissivity, but there is also a significant decrease in deformation zone transmissivity with depth, where the gently dipping zones have the highest transmissivities regardless of elevation followed by the steeply dipping WNW zones.

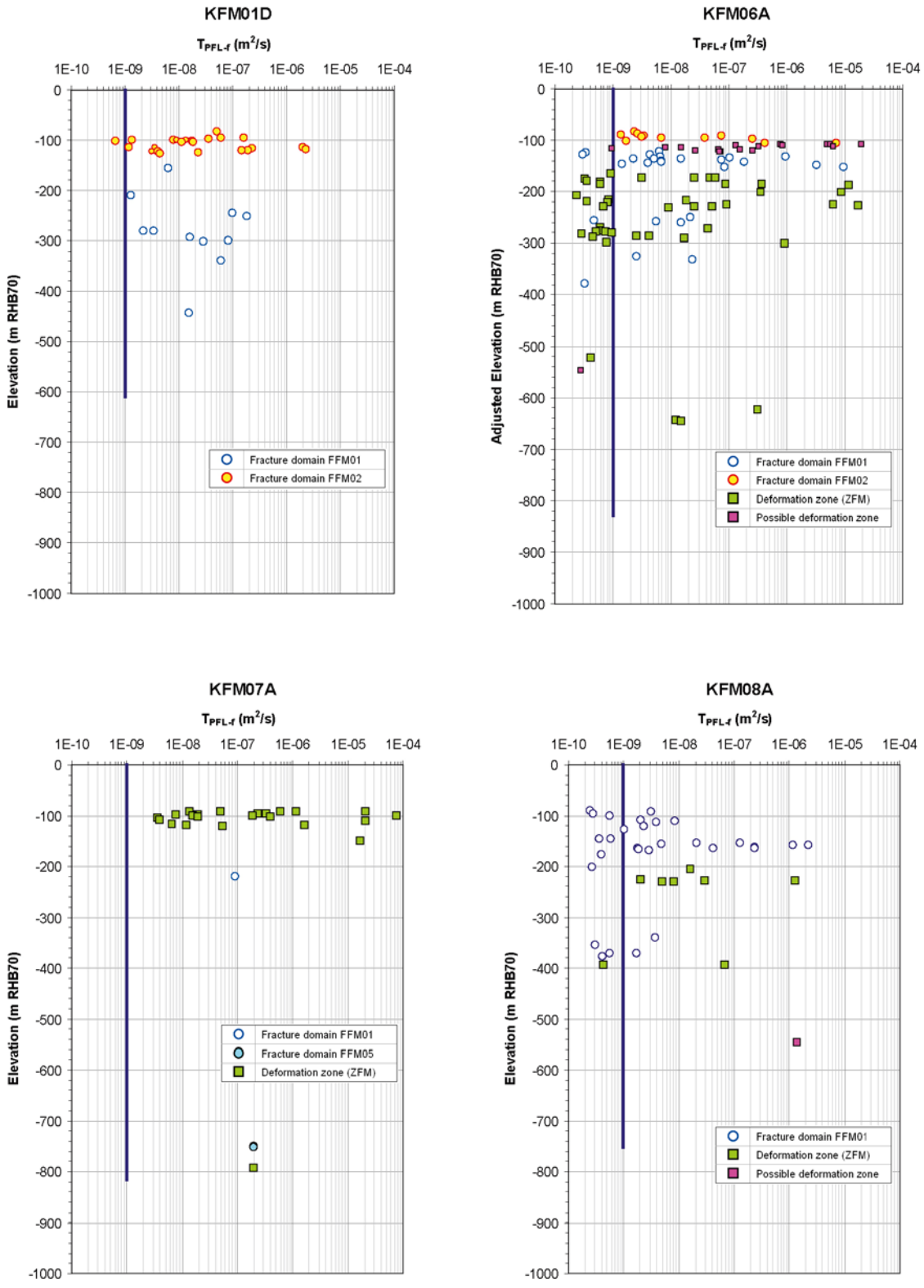

Figure 2-7. *Specific capacity data of flowing fractures in the cored boreholes KFM01D, KFM06A, KFM07A and KFM08A detected with the PFL method. The data are coloured with regard to their structural classification and the blue lines indicate the typical detection limit reported from the investigations in the Forsmark area, 1×10^{-9} m²/s. The lengths of the blue lines correspond to the depths investigated with the PFL method. In Sicada, the specific capacity data determined with the PFL method are called PFL fracture transmissivities, which explains the x-axis caption T_{PFL}.*

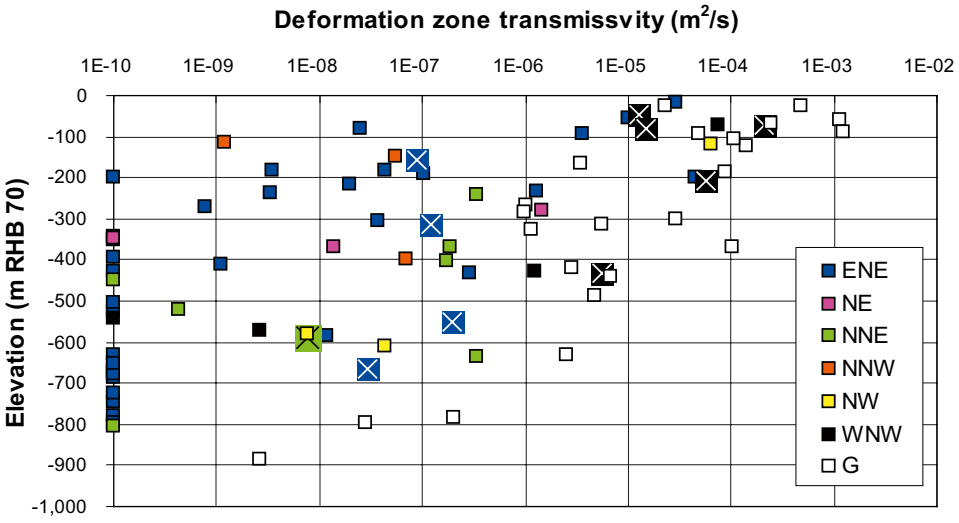

Figure 2-8. *Scatter plot of the in-plane transmissivity data versus depth for the deterministically modelled deformation zones. The transmissivities are coloured with regard to the orientations of the deformation zones. G means gently dipping and the steeply dipping zones are denoted by their strike direction. Data denoted by x come from KFM08D, KFM11A, KFM12A, HFM34, HFM36 and HFM37 and where obtained at the very end of SDM-Site and used for verification (hypothesis testing) purposes, see Follin et al. (2008) for details.*

2.3 Hydraulic characteristics of the fracture domains (HRD)

The hydraulic conductivity estimated from measurements conducted with the PSS method (K_{PSS}) and the Terzaghi corrected conductive fracture frequency and the fracture transmissivity distribution estimated from measurements using the PFL method ($P_{10,PFL,corr}$) are also used to describe the permeability of the rock mass volumes between the deterministically modelled deformation zones.

Figure 2-9 shows a cumulative distribution function plot of 151 $\log_{10}(K_{PSS})$ data measured with a packer spacing (test scale[2]) of 20 m in the depth interval –400 to –700 m. Approximately 90% of the PSS data set (151 measurements) have values below –10.4 (or 4×10^{-11} m/s), which is the robust lower measurement limit of the PSS method. This implies a conductivity-thickness product that is consistent with the PFL detection limit.

Figure 2-10 shows all PFL data acquired in the target area/volume in the rock mass volumes between the deterministically modelled deformation zones, see Figure 2-6. Above –200 m, the conductive fracture frequency is much higher than below this elevation. In fact, there are hardly any conductive fractures below –400 m. The decrease in specific capacity (or PFL fracture transmissivity) is not as significant as the decrease in frequency, although the highest PFL transmissivity data are clearly observed above –200 m. These observations are confirmed by the measurements conducted with the PSS method shown in Figure 2-9. (Table 2-1 lists the boreholes that are tested with both methods.)

It is noted that the PFL data occurring around –450 m are observed in the cored borehole KFM02A at drillsite 2, see Figure 2-1 and the lower image in Figure 2-5. This segment of KFM02A intersects the rock mass volume sandwiched in between two deformation zones, ZFMA2 and ZFMF1, and is not part of the planned repository volume. In conclusion, the fractured rock mass volumes between the deterministically modelled deformation zones look very different above and below approximately –400 m elevation.

[2] A telescopic approach is used for the single-hole hydraulic testing with the PSS method at Forsmark. Each borehole is measured with consecutive 100-m long, 20-m long and 5-m long packer intervals beginning with the longest packer interval. However, non-flowing 100-m long packer intervals are not studied with 20-m long packer intervals, etc. The telescopic measurement approach saves time but it assumes that low-transmissive sections are correctly characterized. To display a cumulative plot of all 20-m sections a uniform distribution of transmissivity (T) is assumed in each low-transmissive 100 m section and the corresponding five unmeasured 20m sections are a assigned a hydraulic conductivity (K) as follows: $K_{PSS,20m} = T_{100m}/5/20$ m.

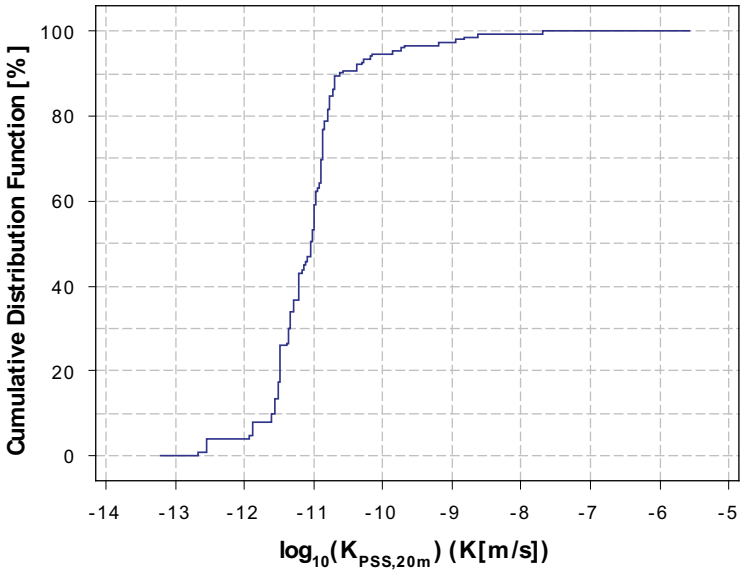

Figure 2-9. *Cumulative distribution plot of 151 $log_{10}(K_{PSS})$ data measured with a packer spacing (test scale) of 20 m between elevations –400 m to –700 m within the target area/volume at Forsmark. The robust lower measurement limit of the PSS method is 4×10^{-11} m/s (log(K) = –10.4).*

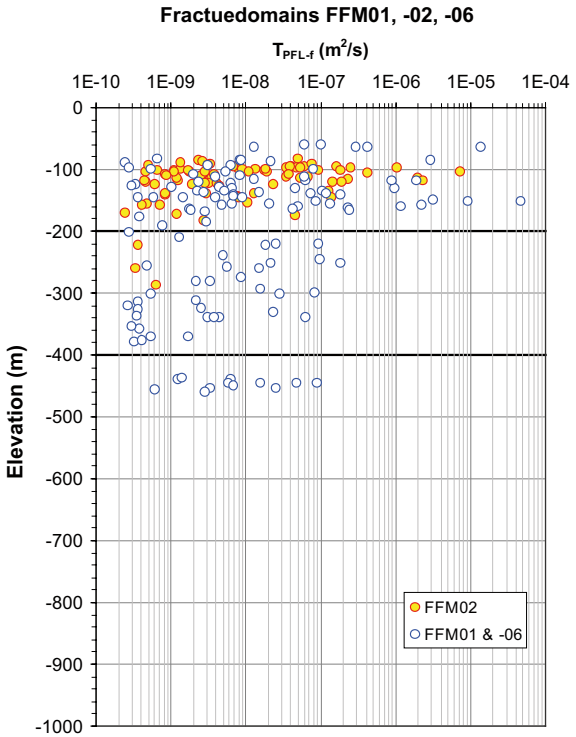

Figure 2-10. *Specific capacity data of the flowing fractures detected with the PFL method in boreholes KFM01A, -01D, -02A, -04A to -08A, -08C and -08D outside deformation zones within the target area/volume (fracture domains FFM01–02 and -06). In Sicada, the specific capacity data determined with the PFL method are called fracture transmissivity data, which explains the x-axis caption T_{PFL}.*

Figure 2-11 shows two types of Terzaghi[3] corrected fracture frequencies in the target area/volume; open fractures (fractures that have visible apertures) and flowing fractures detected with the PFL method. Figure 2-11 shows also the measured specific capacities of the flowing fractures. At repository depth, the geometric mean of the Terzaghi corrected frequency of flowing fractures detected with the PFL method is very low, approximately 0.005 fractures per metre (5/km). The geometric mean of the specific capacity is also low, approximately 6.5×10^{-9} m^2/s. The product of these two values suggest an equivalent hydraulic conductivity of approximately 3.3×10^{-11} m/s for 200-m blocks of rock located below –400 m elevation.

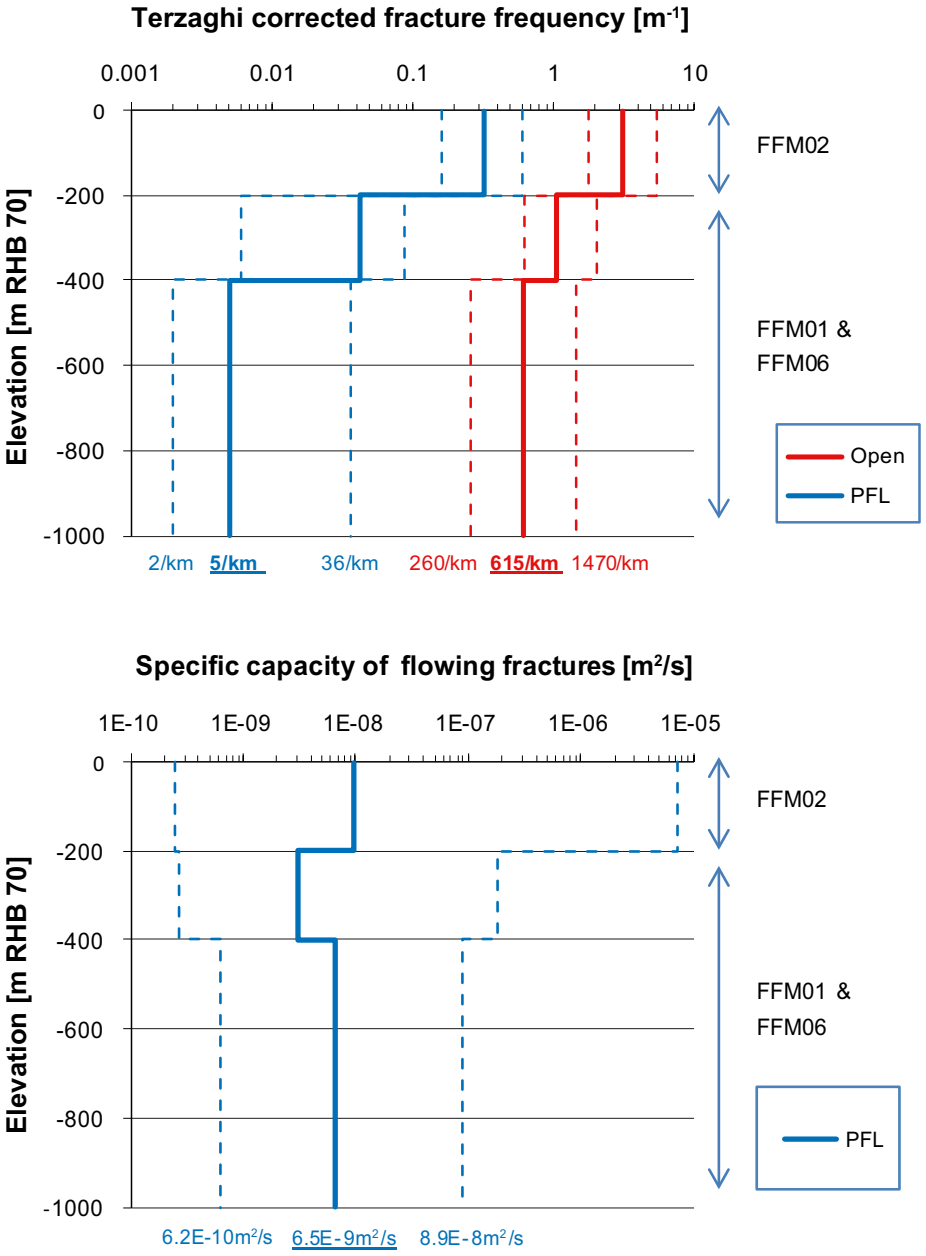

Figure 2-11. *Top: Terzaghi corrected frequencies of open fractures and of the flowing fractures detected with the PFL method. Bottom: Specific capacities of the flowing fractures detected with PFL method. The thicker lines represent the geometric means over all boreholes and the thinner lines represent the spread between individual boreholes, i.e. the minimum and maximum values observed in any borehole.*

[3] Terzaghi correction is a common method used to mitigate orientation bias.

3 Primary data

3.1 Fracture transmissivity

The hydrogeological data used for the analyses reported here represent specific capacity values recorded at fracture intersections in deep cored boreholes. The boreholes are tested with the Posiva Flow Log tool while being pumped as line sinks at presumably steady-state flow conditions. This evaluation is based on the assumption of a cylindrical flow regime and connectivity to a constant head water source (positive hydraulic boundary).

The Posiva Flow Log (Figure 3-1) is a difference flow logging device, which means that the flow rate at each intersecting, flowing fracture is measured twice; first at natural head conditions and second at lowered head conditions. The difference in flow rate, ΔQ [L^3T^{-1}], is divided by the difference in head, Δh [L], and the ratio defines the specific capacity, $\Delta Q/\Delta h$ [L^2T^{-1}], at the fracture intercept. The applied head difference is of the order of 10 m (c. 100 kPa) and the spatial resolution of the Posiva Flow Log device is 0.1 m.

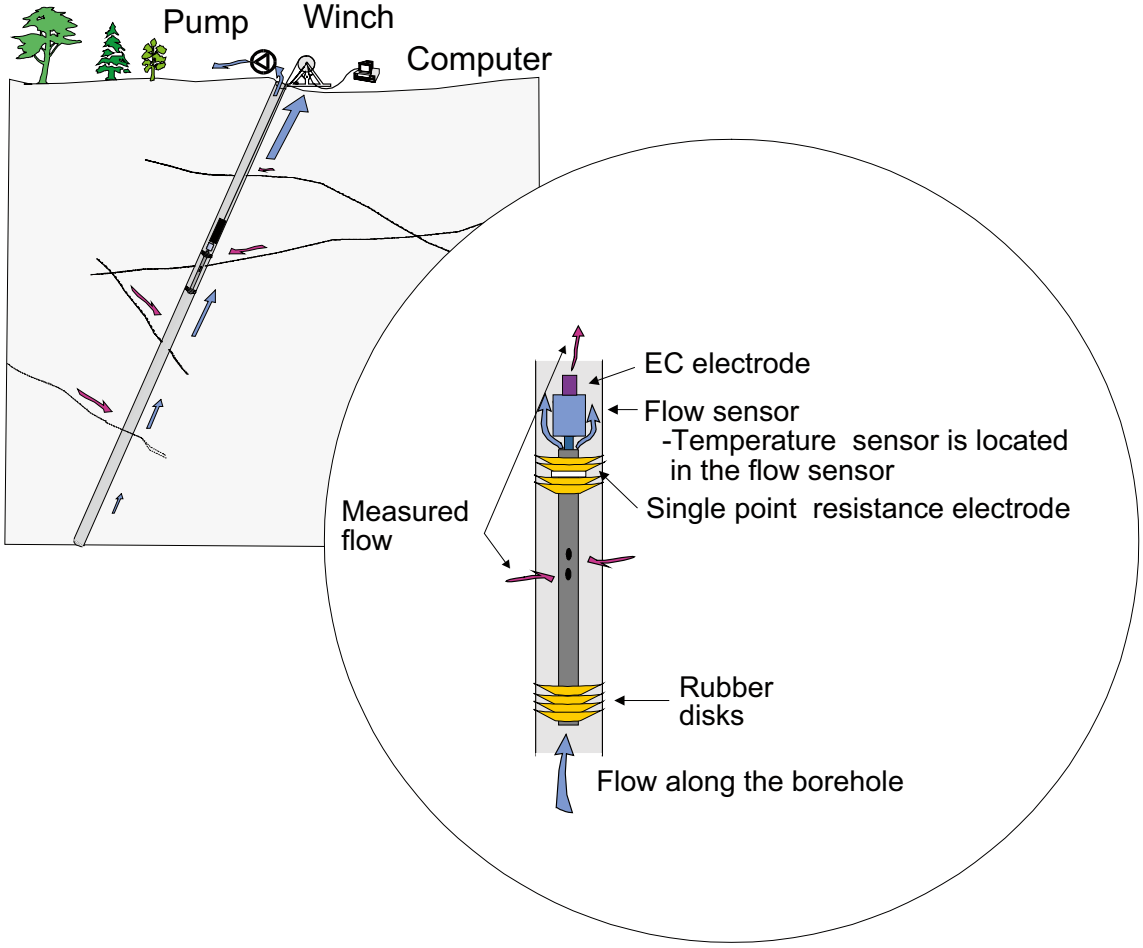

Figure 3-1. *Schematic drawing of the down-hole equipment used for difference flow logging in Forsmark. Reproduced from Rouhiainen and Sokolnicki (2005).*

In SKB's database, Sicada, the specific capacity at an intersecting flowing fracture determined with the PFL method is called fracture transmissivity, T [L^2T^{-1}]. The transformation from specific capacity to transmissivity is made by the investigator, who uses Thiem's well equation (Thiem 1906):

$$T = (Q/\Delta h)\ [\ln(r_e/r_w) / 2\pi] \qquad (3\text{-}1)$$

where r_e [L] is the radius of influence of the hydraulic test and r_w[L] is the nominal radius of the cored borehole (approximately 0.0385 m). The results reported to Sicada are based on the assumption that the ratio of r_e/r_w is constant along the borehole and equal to 500. Hence, the value of the term between the square brackets is set to unity and Equation 3-1 becomes:

$$T \approx Q/\Delta h \qquad (3\text{-}2)$$

In other words, the values reported to Sicada are specific capacities. The PFL transmissivity value reported to Sicada will be close to the local value at the borehole (i.e. the transmissivity of the intersecting flowing fracture) if the local value is less than the overall transmissivity of the network to which is connected. If the local value at the borehole is greater than the overall transmissivity of the network to which is connected, the PFL transmissivity value determined by Equation 3-2 represents a "hydraulic choke" (bottleneck) phenomenon, which means that it is not the transmissivity of the intersecting flowing fracture that is determined, see Follin et al. (2011) for details.

3.2 Fracture orientation

The orientations of the intersecting, flowing fractures are determined by comparing their positions in the boreholes with the positions of the open fractures identified during the core mapping (Boremap) and the viewer logging (BIPS).

Figure 3-2 shows an example of a BIPS image recorded in borehole KFM01D located in the centre of the target volume, see Figure 2-1. The fracture marked by the red arrow is located at a borehole length of 316.96 m and has a strike of 110°, dip of 12°, visible aperture of 3 mm and a specific capacity, or Sicada PFL fracture transmissivity, of 1.83×10^{-7} m^2/s.

The important work of correlating PFL data to fracture geometry data is carried out by Forssman et al. (2004, 2008) and Teurneau et al. (2008).

3.3 In situ stress

The in situ normal stress acting on each fracture used for the analyses reported here are determined using the in situ stress gradients given in Glamheden et al. (2007). The analyses, unless otherwise indicated, is restricted to the target volume, i.e. the rock volume that has been identified as suitable for the excavation of the high-level radioactive waste repository, see Figure 2-1.

The recommended in situ stress gradients versus depth at Forsmark are given in Table 3-1 and Figure 3-3.

Table 3-1. Recommended horizontal and vertical stress magnitudes for the Forsmark target area, where the depth below surface is d in metres. A depth of 0 is approximately equal to an elevation of 0 m (Glamheden et al. 2007).

Depth [m]	Maximum horizontal stress, σ_{1H} [MPa]	Trend [°]	Minimum horizontal stress, σ_{2h} [MPa]	Trend [°]	Vertical stress σ_{3v} [MPa]
0–150	19+0.008d ±20%	145±20	11+0.006d ±25%	055	0.0265d ±2%
150–400	9.1+0.074d ±15%	145±15	6.8+0.034d ±25%	055	0.0265d ±2%
400–600	29.5+0.023d ±15%	145±15	9.2+0.028d ±20%	055	0.0265d ±2%

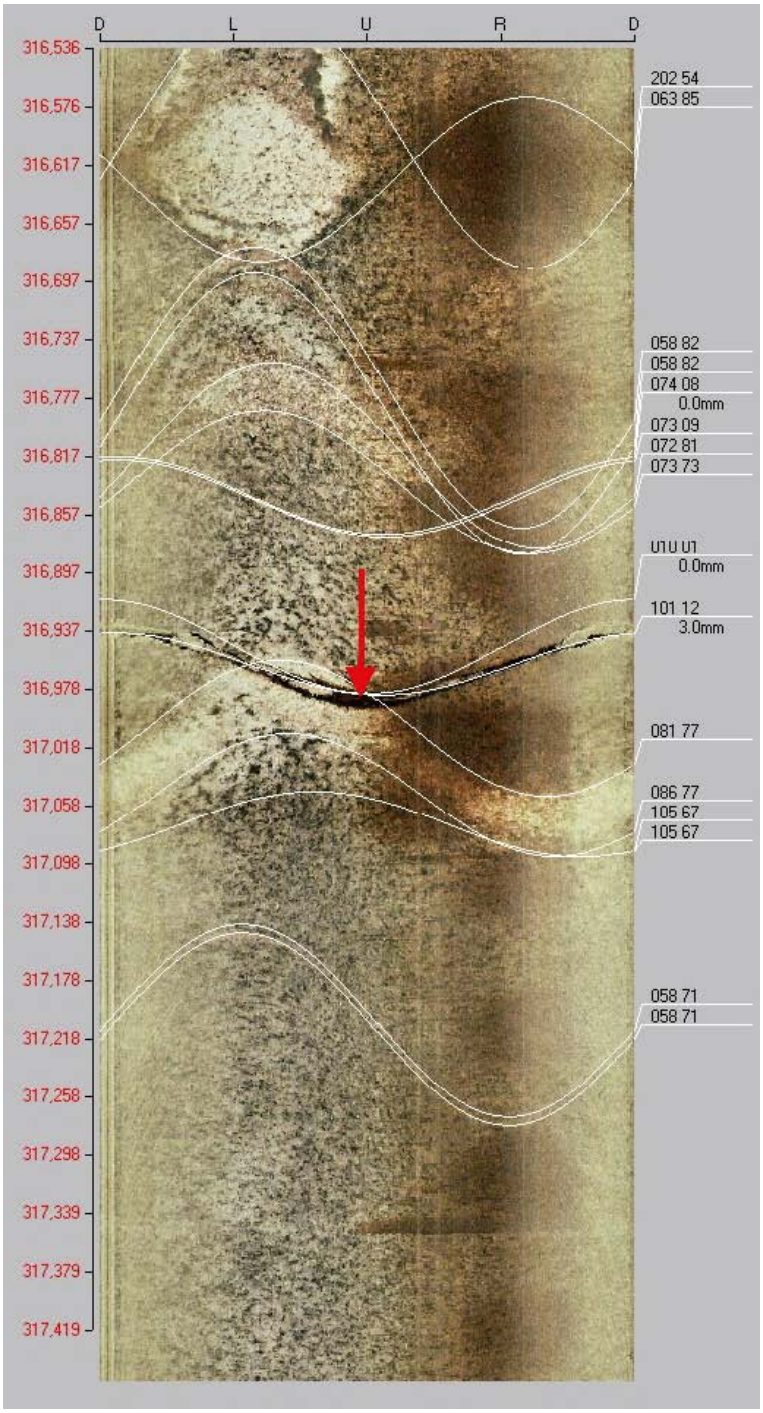

Figure 3-2. *Example of the structural interpretation of PFL feature no. 27 recorded in borehole KFM01D (Teurneau et al. 2008). The total length of the image is 0.88 m. The fracture marked by the red arrow is located at a borehole length of 316.96 m and has a strike of 101°, dip of 12°, visible aperture of 3 mm and a specific capacity, or Sicada PFL fracture transmissivity, of 1.83×10^{-7} m^2/s.*

Table 3-1 implies that the very transmissive gently dipping deformation zones, see Figure 2-3 and Figure 2-8, are at a high angle to the minimum principal stress (σ_{3v}) and at a low angle to the azimuths of both the first (σ_{1H}) and second principal stresses (σ_{2h}). Further, the deformation zones that strike WNW-NW are at low angle to the azimuth of σ_{1H} , whereas the opposite condition prevails for the deformation zones that strike NNE-ENE, see Figure 2-2. The observation made in Figure 2-8 is that the former set of zones is more transmissive than the latter set.

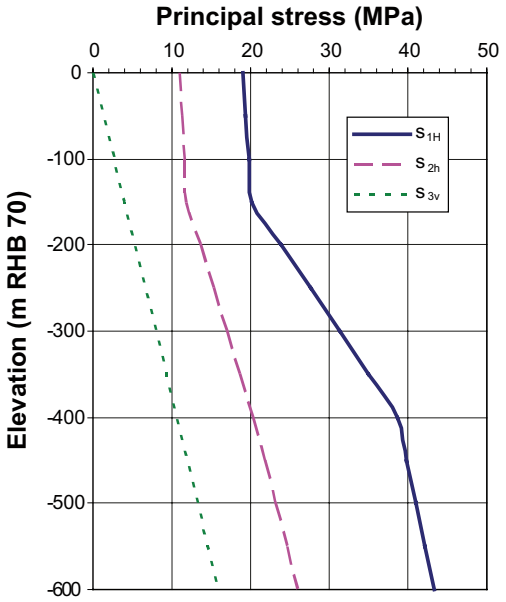

Figure 3-3. *Plot of the in situ stress gradients versus depth at Forsmark as given in the work by Glamheden et al. (2007).* σ_{1H}*=Maximum horizontal stress,* σ_{2h}*= minimum horizontal stress and* σ_{3v}*=vertical stress. All principal stresses increase with depth.*

3.4 Assumptions

The work reported here assumes that the specific capacity values measured with the PFL method and reported to Sicada as PFL fracture transmissivity data represent the local transmissivity values at the borehole, i.e. the transmissivity of the intersecting flowing fractures. Second, it is assumed that the correlation analyses carried out by Forssman et al. (2004, 2008) and Teurneau et al. (2008) give the correct fracture orientations. Third, the analysis of PFL for stress analysis is divided into three hydrogeological categories:

1. **ALL_PFL**: This data set is used to assess the general trend in all PFL data, i.e. both inside and outside the target volume regardless of spatial location or geological context. It consists of 613 PFL data.
2. **FFM_PFL**: This data set is used to assess the trend in the PFL inside the target volume, i.e. data spatially distributed within fracture domains FFM01, FFM02, and FFM06. It consists of 271 PFL data.
3. **ZFM_PFL**: This data set is used to asses the trend in 70 deterministically modelled deformation zones that occur inside or in close proximity to the target volume. Transmissivity values of deterministically modelled deformation zones are obtained by adding all individual values between the defined geometrical bounds of each deformation zone. Deformation zones with little or no flow have been assigned an arbitrary low transmissivity value of 1×10^{-10} m^2/s, see Figure 2-8. The 70 deformation zones have been assigned the following orientation categories: G (gently dipping; 13), ENE (36), NE (3), NNE (8), NNW (3), NW (3), and WNW (4).

Table 3-1 reveals that the minimum stress is vertical, the intermediate stress is the minimum horizontal stress (Azimuth 55°) and the maximum stress is the maximum horizontal stress (Azimuth 145°). Hence, hydrogeological features that are oriented in these directions offer the greatest potential to observe possible relations between fracture flow and stress. In the analyses which follow the data have been divided into three orientation categories:

1. Sub-horizontal (dip ≤ 20°).
2. NE-SW: Steeply dipping (dip ≥ 60°) with a strike between Azimuth 0° and 90° and between Azimuth 180° and 270°.
3. NW-SE: Steeply dipping (dip ≥ 60°) with a strike between Azimuth 90° and 180° and between Azimuth 270° and 360°.

4 In situ stress vs PFL fracture transmissivity

4.1 Frequency of PFL fracture transmissivity data

Figure 4-1 shows a histogram of 613 PFL fracture transmissivity data recorded at Forsmark. The lower detection limit of the PFL tool is approximately 10^{-9} m^2/s. Figure 4-2 shows that the number of PFL fracture transmissivity data decreases significantly with depth. It is noted that the average vertical depth of the 13 boreholes providing PFL fracture transmissivity data to the present work is – 813 m.

4.2 Analysis of ALL_PFL

This data set contains 613 PFL fracture transmissivities. The data are not restricted spatially or geologically, i.e. no filtering has been applied to the data.

The upper left figure in Figure 4-3 shows a lower hemisphere stereonet plot of the fracture poles. Many of the fracture orientations are sub-horizontal. The upper right figure in Figure 4-3 shows and the distribution with depth. The normal stress acting on each fracture is determined using the stress gradients and orientations given in Glamheden et al. (2007) and Follin et al. (2007a), respectively. The result from these stress calculations are shown in the lower left figure. A trend line is established for the relation between normal stress and PFL fracture transmissivity using Equation 1-2, see the lower right figure in Figure 4-3. The fitted trend line is based on a moving median of the original data. The fitted trend line is also plotted on the original data for comparative purposes; see the lower left figure in Figure 4-3.

4.3 Analysis of FFM_PFL

This data set contains 193 PFL fracture transmissivities found in fracture domains FFM01, FFM02 and FFM06. These fracture domains are considered representative of the target volume. The analysis procedure described for the ALL_PFL data set in Section 4.2 is applied to the FFM_PFL data set. The results of the analysis are shown in Figure 4-4 through Figure 4-7.

4.4 Analysis of ZFM_PFL

This data set contains 70 deterministically modelled deformation zones that occur inside the target volume or in close proximity to the target volume. The analysis procedure described for the ALL_PFL data set in Section 4.2 is applied to the ZFM_PFL data set. The results of the analysis are shown in Figure 4-8 through Figure 4-11.

Although it is known that the orientation of the stress tensor in Table 3-1 is valid as a regional orientation, there is uncertainty in the stress magnitudes outside the target area. The analyses given below should be viewed noting this limitation.

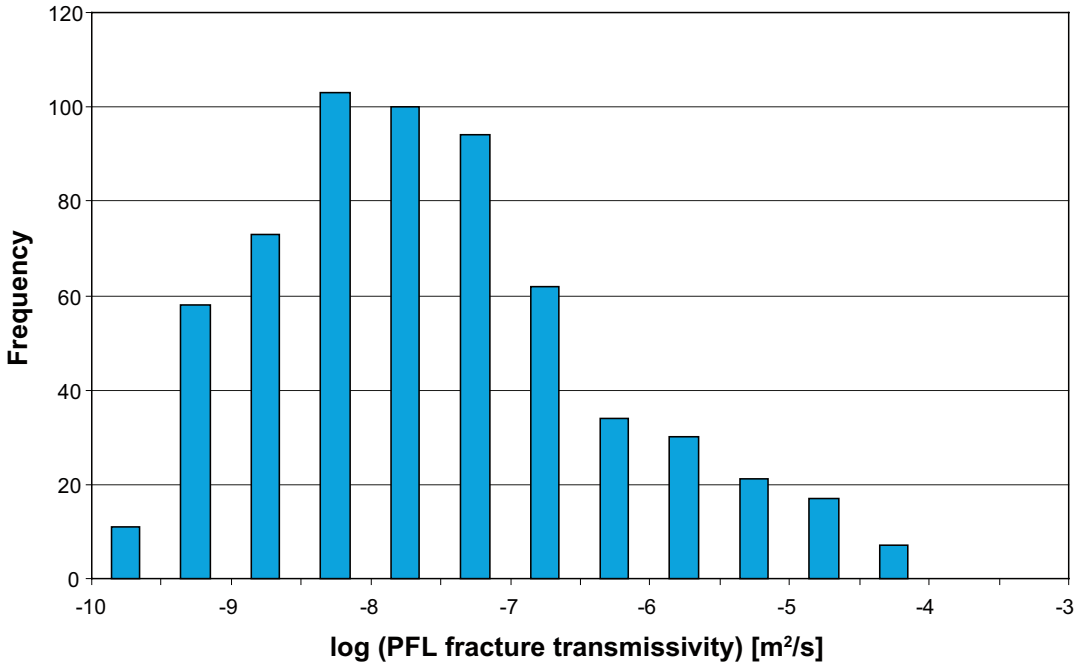

Figure 4-1. *Histogram of all PFL fracture transmissivity data used in the work reported here.*

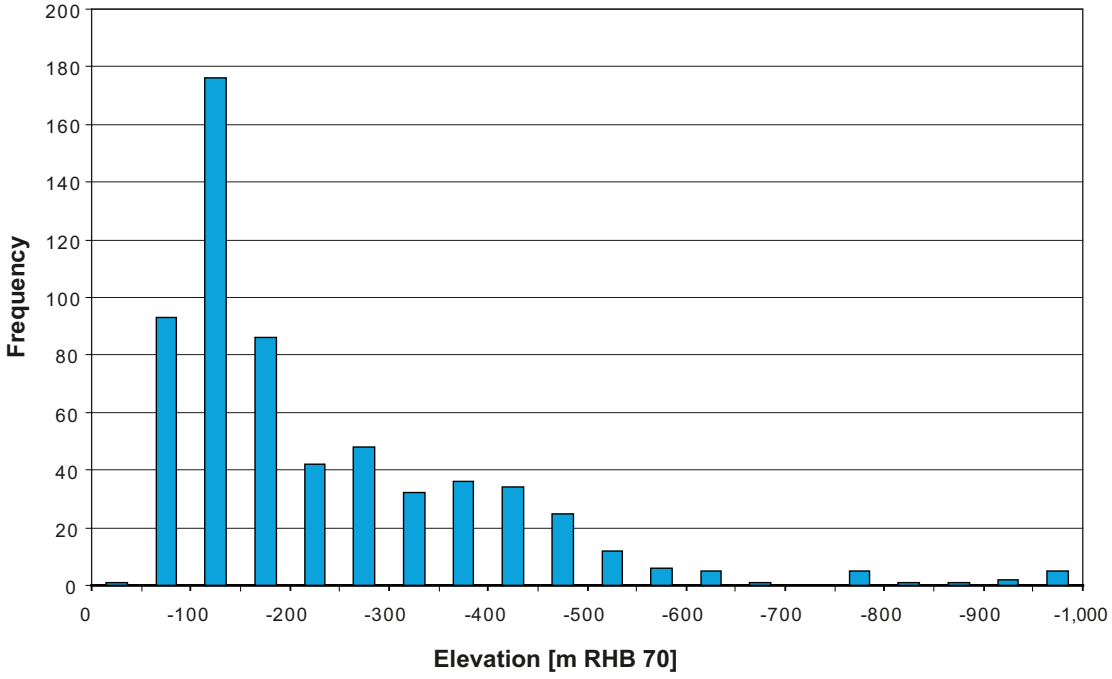

Figure 4-2. *Histogram of the 613 PFL fracture transmissivity data versus depth. (RHB 70 is short for the Swedish Ordnance Datum used.)*

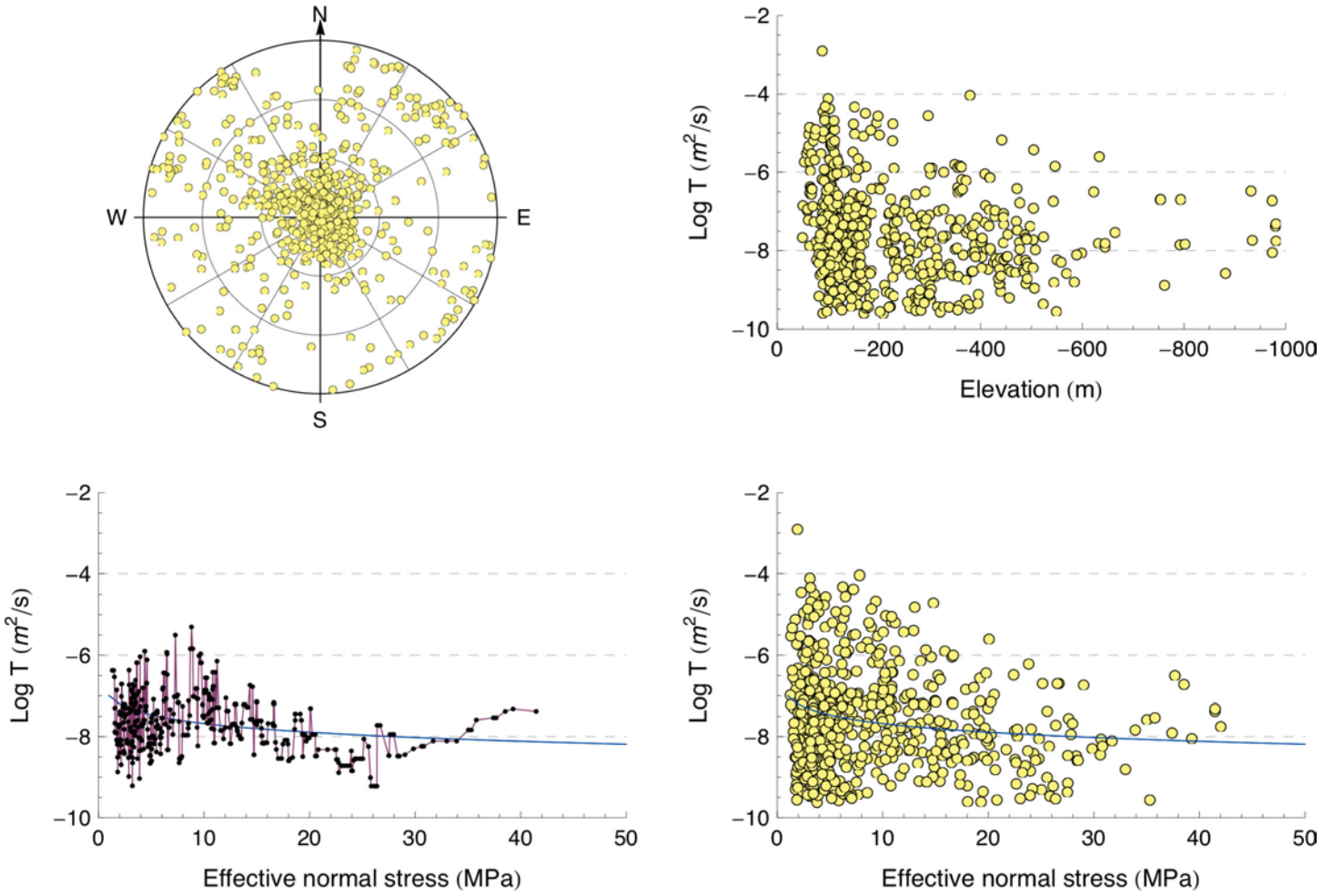

Figure 4-3. *Analysis of the ALL_PFL data set with regard to depth and the normal stress acting on these data (N=613). The trend in the data shown in the lower right figure is established using a moving median technique and Equation 1-2.*

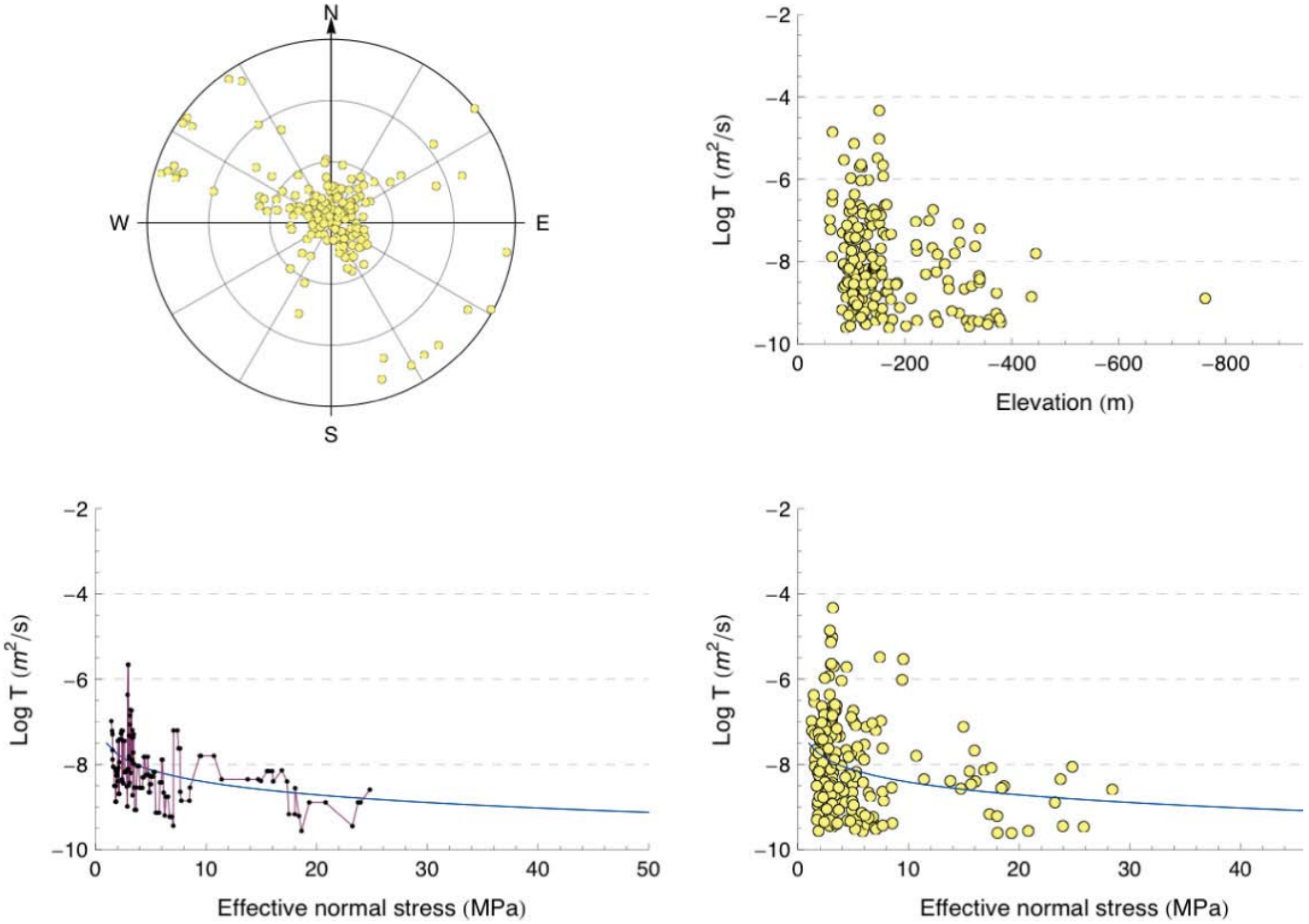

Figure 4-4. *Analysis of the FFM_PFL data set with regard to depth and the normal stress acting on these data (N=193). The trend in the data shown in the lower right figure is established using a moving median technique and Equation 1-2.*

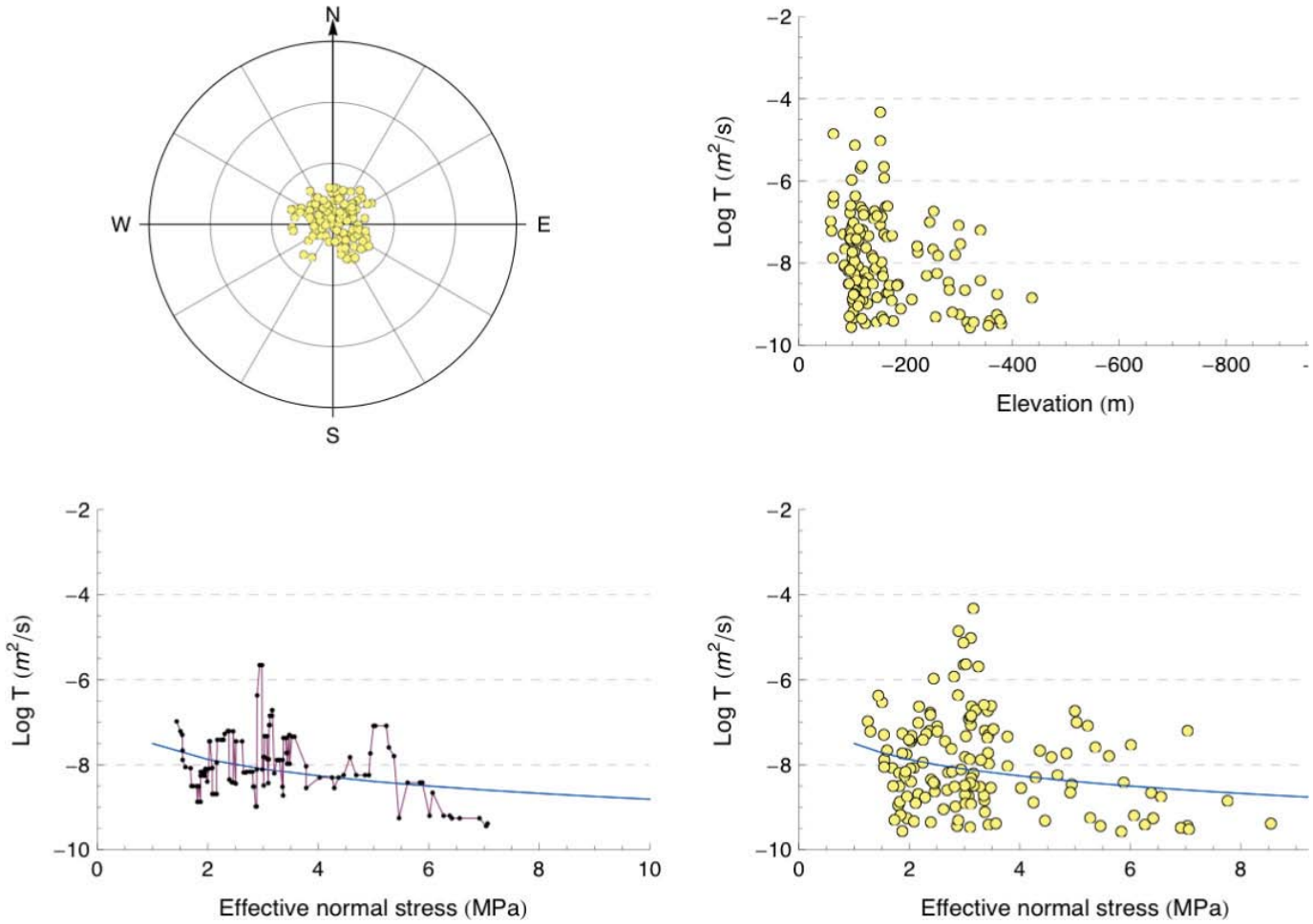

Figure 4-5. *Analysis of the gently dipping fractures within the FFM_PFL data set (N=140) with regard to depth and the normal stress acting on these data. The trend in the data shown in the lower right figure is established using a moving median technique and Equation 1-2.*

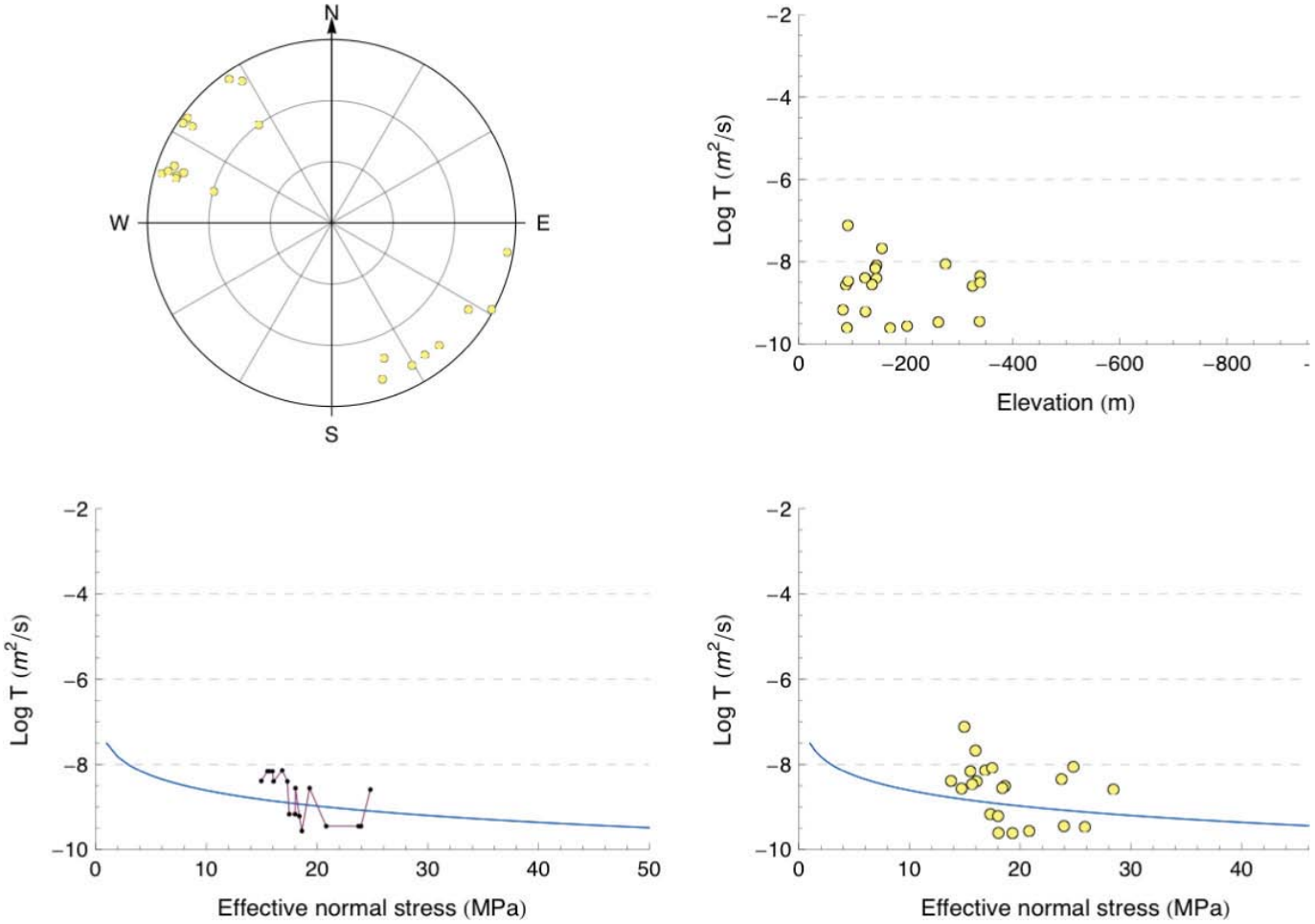

Figure 4-6. *Analysis of the NE-SW steeply dipping fractures within the FFM_PFL data set (N=21) with regard to depth and the normal stress acting on these data. The trend in the data shown in the lower right figure is established using a moving median technique and Equation 1-2.*

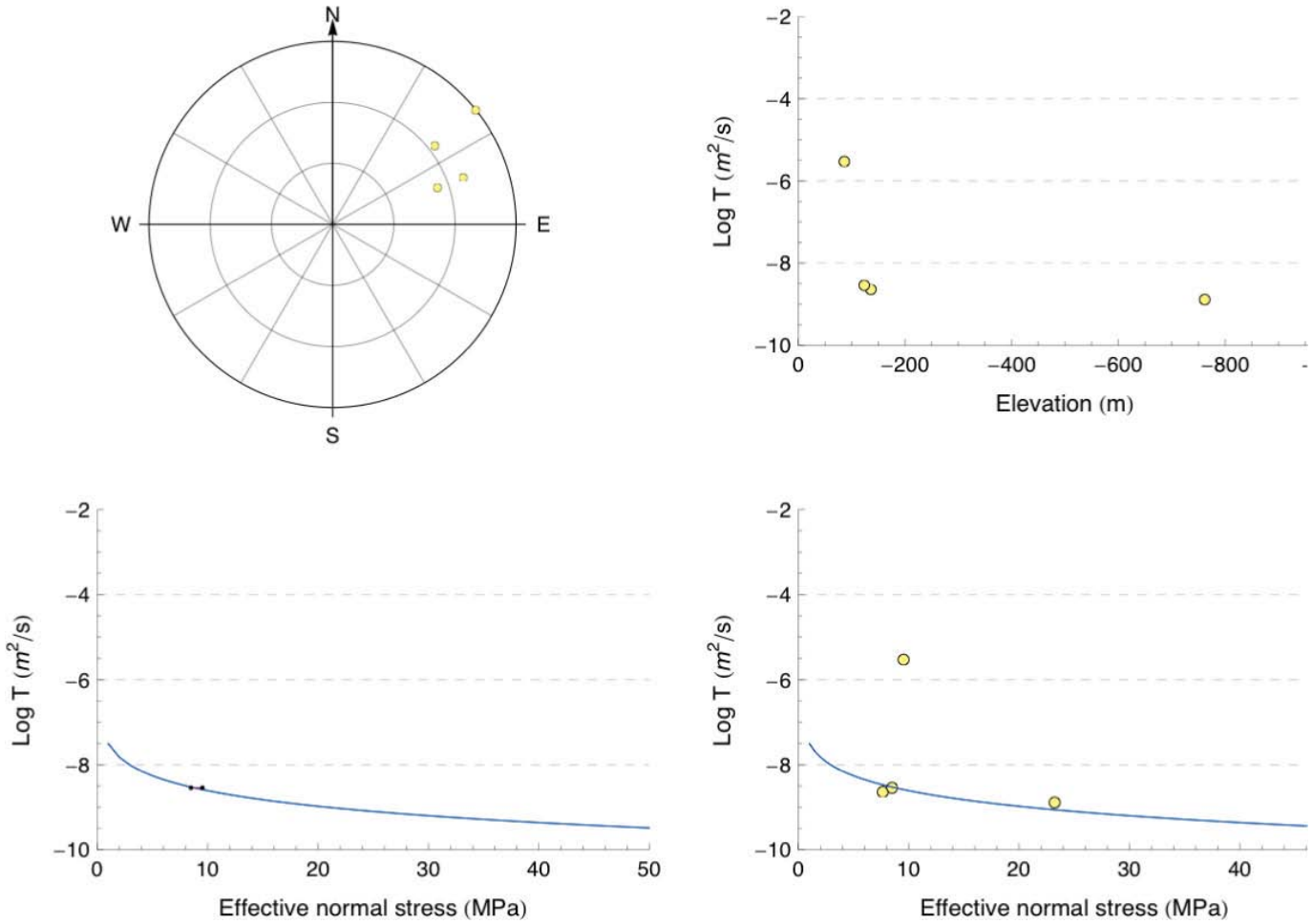

Figure 4-7. *Analysis of the NW-SE steeply dipping fractures within the FFM_PFL data set (N=4) with regard to depth and the normal stress acting on these data. The blue trend line was established using Equation 1-2.*

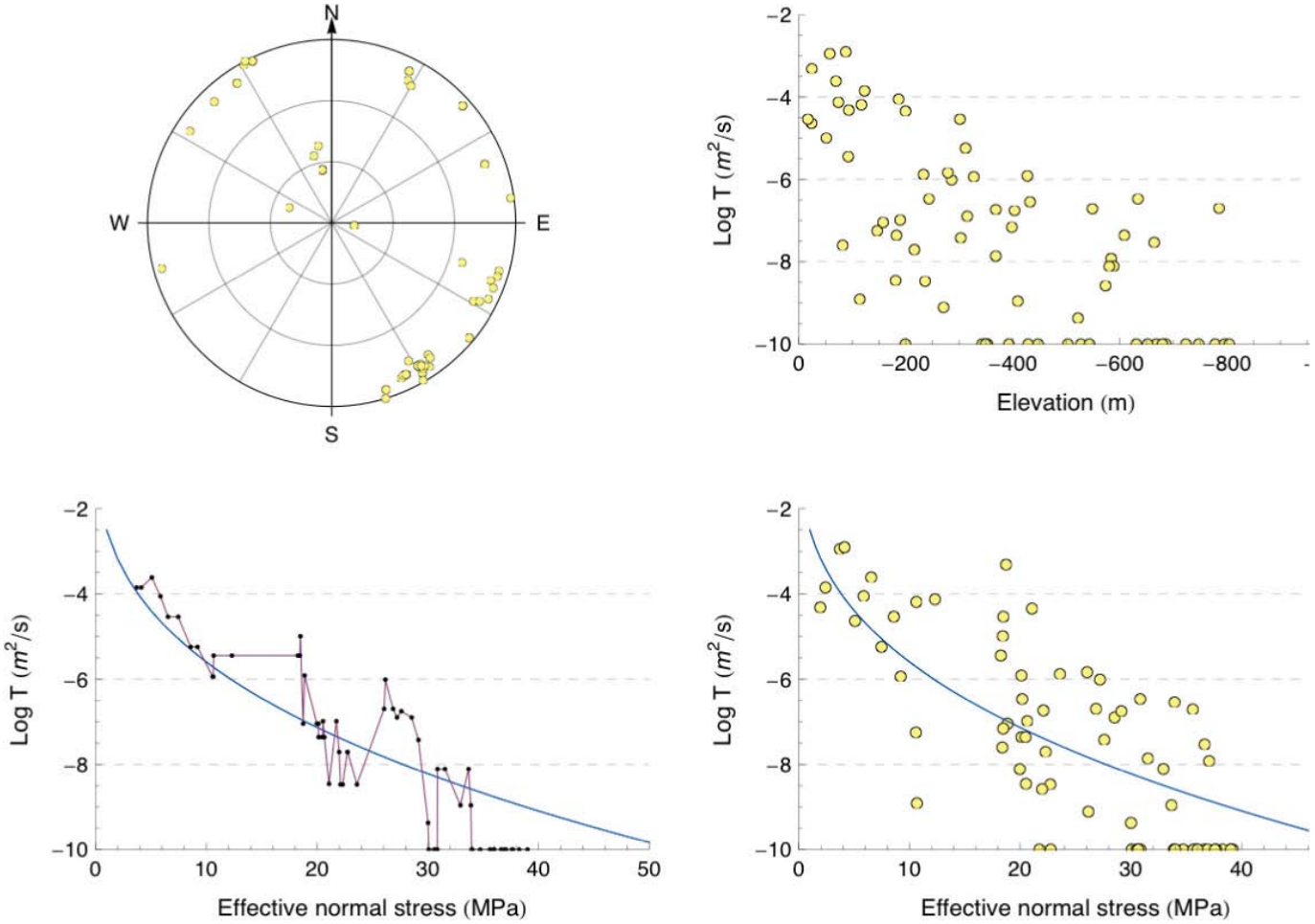

Figure 4-8. *Analysis of the ZFM_PFL data set with regard to depth and the normal stress acting on these data (N=70). The trend in the data shown in the lower right figure is established using a moving median technique and Equation 1-2.*

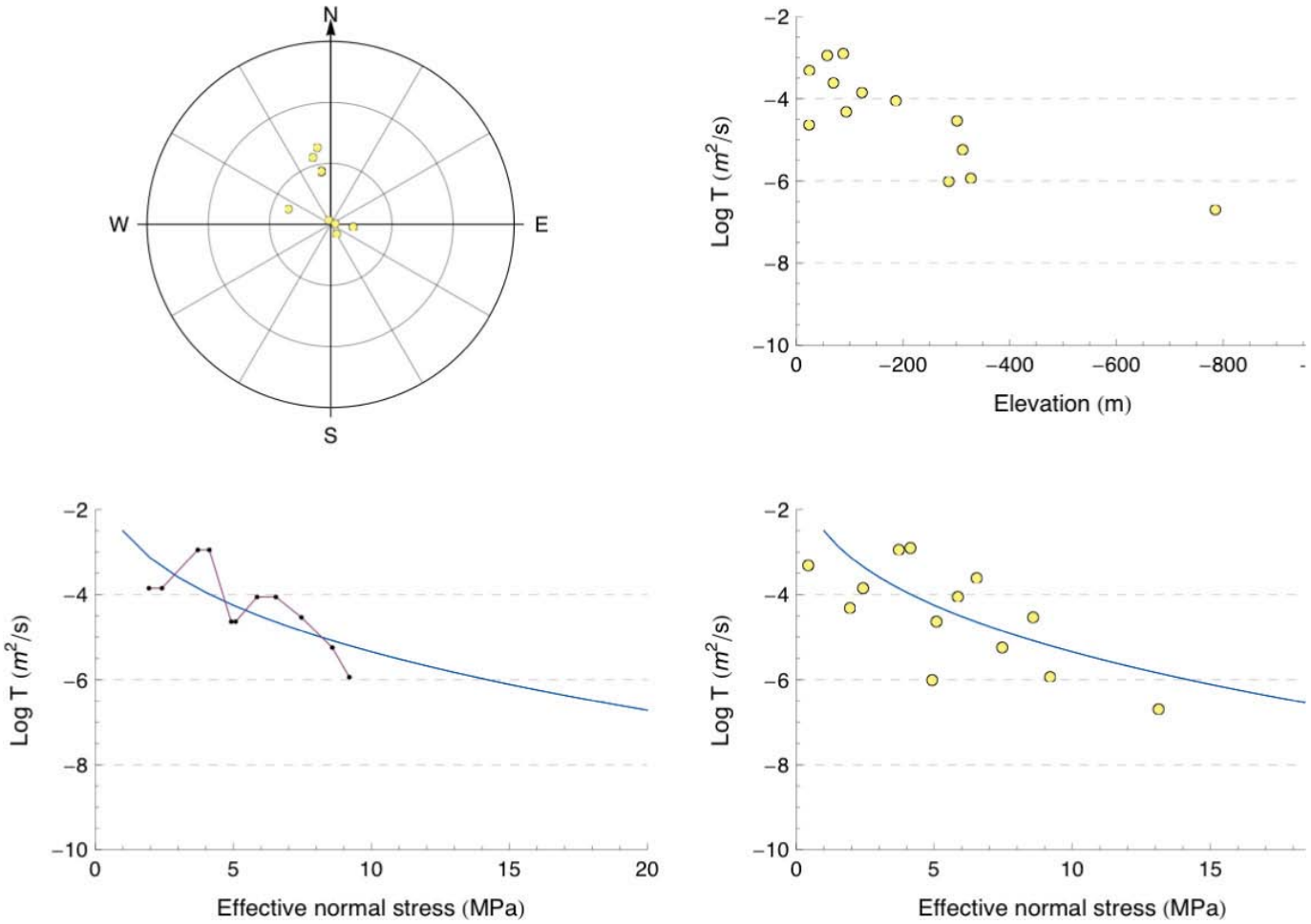

Figure 4-9. *Analysis of the gently dipping zones within the ZFM_PFL data set with regard to depth and the normal stress acting on these data (N=13). The trend in the data shown in the lower right figure is established using a moving median technique and Equation 1-2.*

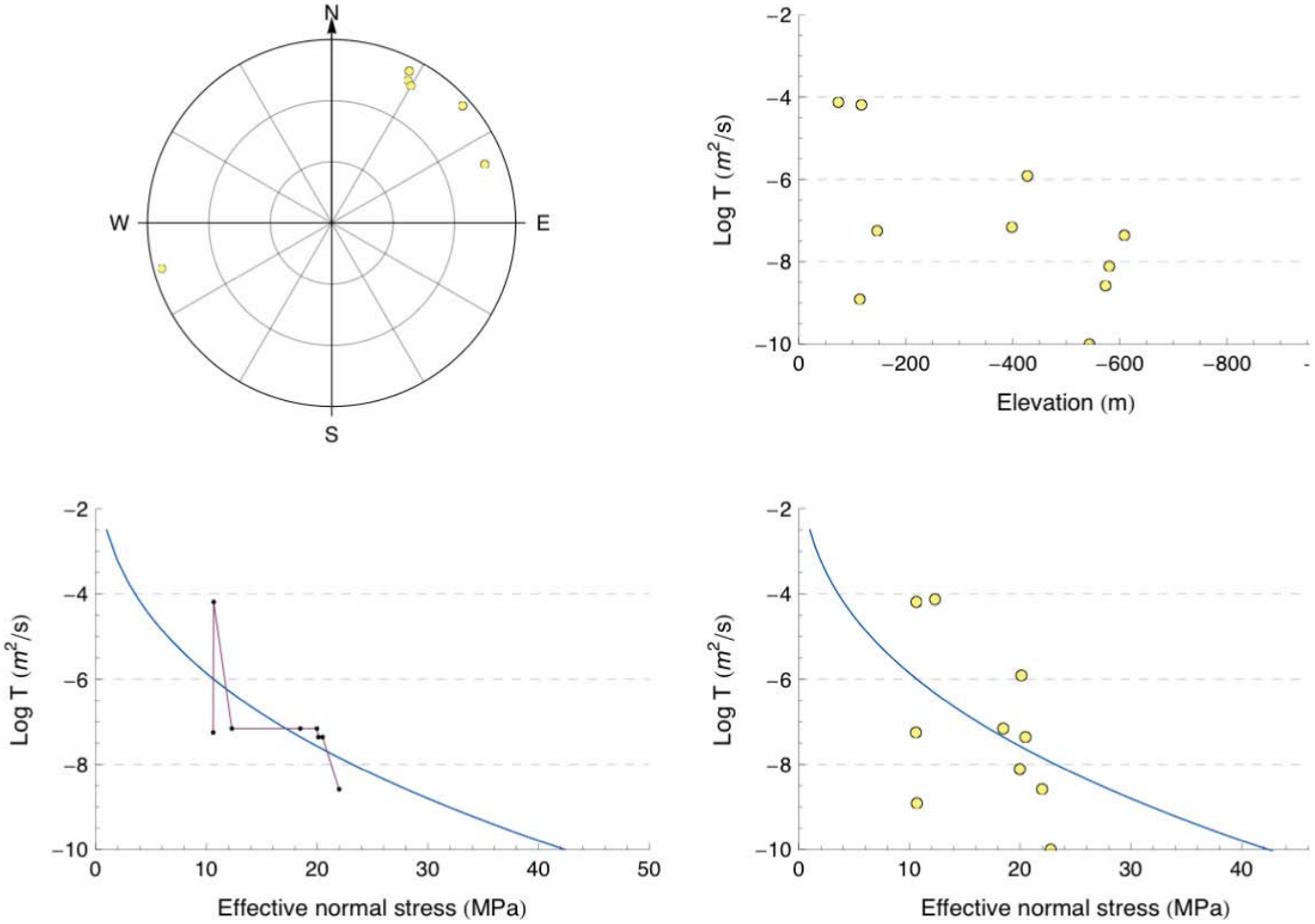

Figure 4-10. *Analysis of the NW-SE steeply dipping zones within the ZFM_PFL data set with regard to depth and the normal stress acting on these data (N=10). The trend in the data shown in the lower right figure is established using a moving median technique and Equation 1-2.*

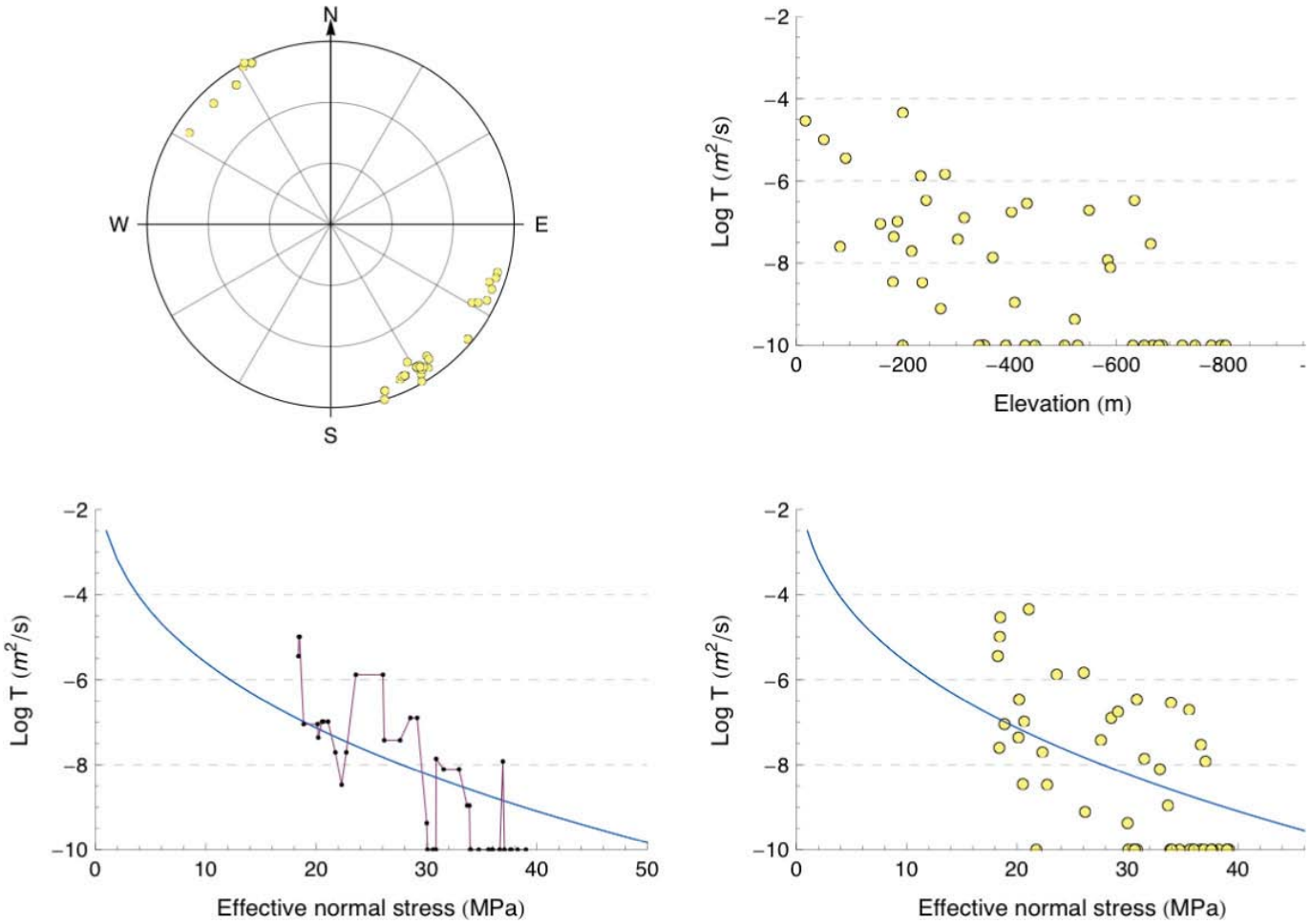

Figure 4-11. *Analysis of the NE-SW steeply dipping zones within the ZFM_PFL data set with regard to depth and the normal stress acting on these data (N=46). The trend in the data shown in the lower right figure is established using a moving median technique and Equation 1-2.*

5 Influence of dilation and slip on fracture transmissivity

5.1 Theory

The progressive fracture of a rock due to the application of a deviatoric stress is a complex process that usually results in a shear zone (deformation zone) caused by strain localisation. Detailed characterisation of this process by Cloos (1955) showed that the shear zone is made up of series of discrete fractures forming at various angles to the direction of shearing. The initiation of this strain localisation generally results in the formation of extensional fractures (see Figure 5-1). These extensional fractures form normal to the minimum principal stress and if the stress state remains unchanged, they may remain open. However, if the stress state changes these fractures may close due to application of a normal stress. The opening or dilation potential (D) for a fracture surface can be expressed as:

$$D = (\sigma_1 - \sigma_n) / (\sigma_1 - \sigma_3) \quad (5\text{-}1)$$

where σ_n = normal effective stress (Pa) acting on the fracture, σ_1 = major effective principal stress (Pa), and σ_3 = minimal effective principal stress (Pa).

D can vary between 0 and 1 and a fracture with a $D = 0$ has the lowest potential for dilation, whereas a fracture with a $D = 1$ has the highest potential of being open.

The final stages of strain localisation results in shear displacements and the formation of the principal slip surface (Skempton 1966). In order for fractures to slip their orientation relative to the in situ stress state must be such that the shear stress developed on the existing fracture equals the fracture shear strength (Figure 5-1). To evaluate the potential for fracture slip, a simple slip criterion (S) for a purely frictional fracture can be expressed as:

$$S = \tau / \sigma_n \quad (5\text{-}2)$$

where τ = shear stress (Pa) acting on the fracture and σ_n = normal effective stress (Pa) acting on the fracture.

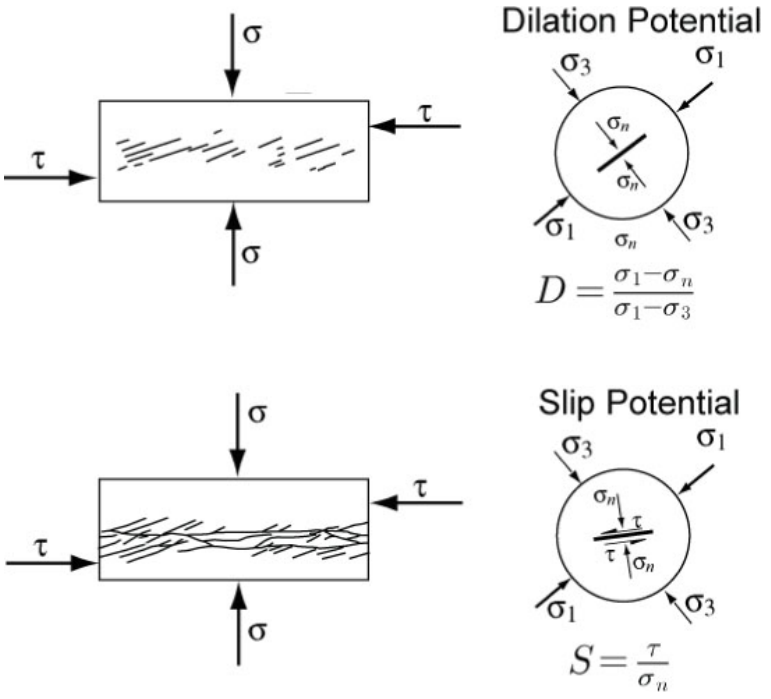

Figure 5-1. *Illustration of the criteria used for assessing the potential for fracture dilation and slip.*

A fracture will slip when S equals the shear strength of the fracture. The shear strength can be expressed as effective stress by incorporating the pore water pressure. It is assumed that once a fracture slips it will also dilate and increase the permeability of the fracture as has been demonstrated in laboratory experiments (Esaki et al. 1995).

Ferrill et al. (1999) used the dilation (D) and slip criterion (S) to identify the orientation of potentially critically stressed fractures relative to in situ stress state to evaluate their permeability potential. Based on groundwater flow studies at Yucca Mountain, Ferrill et al. (1999) suggested a value of $D = 0.8$ as an indicator for potentially dilatant fractures. Rogers (2003) used a similar approach to analyse potential flow paths at Sellafield.

Experimental results in the published literature show that the ratio of normal stress to shear stress required to initiate sliding at low normal stress varies widely between experiments and rock types. Byerlee (1978) suggested that this variability was due to fracture roughness and that at very high normal stress this roughness is reduced significantly and that slip typically occurs when $S \geq 0.6$. Barton et al. (1995) compiled the shear strength for joints in igneous rock and found S ranged 0.6 to 4 depending on the normal stress and rock type.

Glamheden et al. (2008) show that over the normal stress range of 0 to 20 MPa, the peak friction coefficients measured on the open fractures at Forsmark ranged from 0.58 to 0.84. However, the strength of these fractures also had an apparent cohesion, due to small scale roughness, that range from 0.2 to 1.3 MPa. It should also be noted that many fractures have relatively short trace lengths and that rock bridges often separate one fracture from another. Hence, assessing the in situ strength of a fracture at the measured fracture trace length scale or the scale of the hydraulic measurement is very challenging. For the purposes of this evaluation, $S = 0.8$ is taken as a potential indicator of slip and cohesion is ignored.

5.2 PFL fracture transmissivity data in deformation zones

The hydrogeological model at Forsmark is presented in Chapter 2. Fractures in the fracture domains are discrete fractures with relatively short trace lengths as shown in the trace map of the fractures encountered at drillsite 2 (Figure 5-2). The mean trace length of the fractures mapped in the outcrops at Forsmark was 1.3 m. These fractures may be considered similar to the fractures in the top sketch in Figure 5-1. It is highly unlikely that these fractures would be subjected to dilational slip. The deterministically modelled deformations zones mapped at Forsmark, however, appear as discrete zones of intense fracturing (Figure 5-3) similar to that illustrated in the bottom sketch in Figure 5-1. The fractures associated with the deterministically modelled deformation zones may be more susceptible to slip and hence the PFL data within these zones are analysed to determine possible correlations between slip and transmissivity.

The PFL data occurring in the deformation zones are first divided into 3 groups:

1. Gently dipping,
2. NE-SW steeply dipping. and
3. NW-SE steeply dipping

Second, each group of data is evaluated for dilation and slip using the criteria in Equations 5-1 and 5-2, pore pressures and the in situ stress state.

Figure 5-4 shows the potential dilation and slip criteria for all the gently dipping PFL fractures. Figure 5-4 shows that all the fractures have $D > 0.8$ and $S > 0.8$. This suggests that all of the gently dipping PFL fractures should have significantly higher transmissivity values than PFL fractures with $D < 0.8$ and $S < 0.8$.

Figure 5-5 and Figure 5-6 show the dilation and slip potential for the NE-SW and NW-SE steeply dipping PFL fractures, respectively. In contrast to Figure 5-4, Figure 5-5 and Figure 5-6 clearly show that $D << 0.8$ and $S << 0.8$, which implies that the steeply dipping NE-SW and NW-SE PFL fractures should have significantly lower transmissivity values.

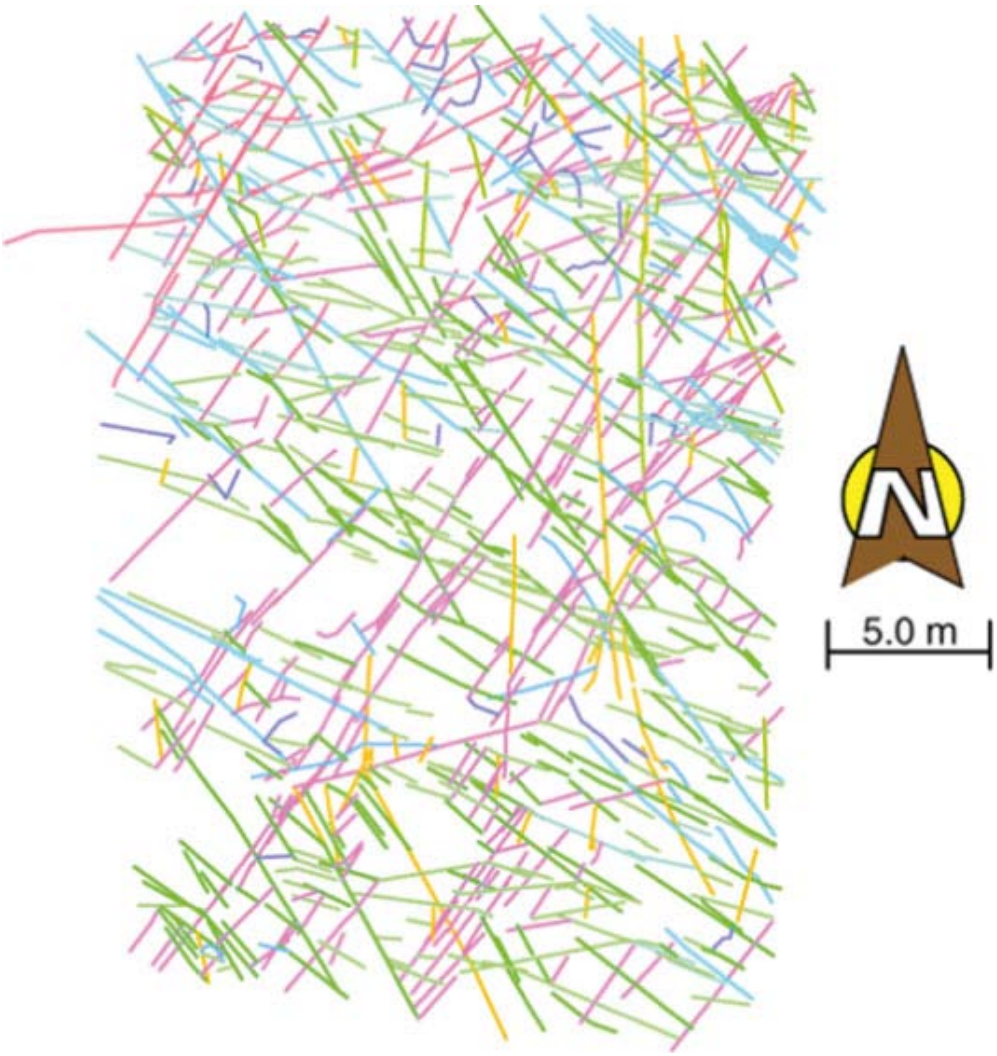

Figure 5-2. *Fracture outcrop map for Forsmark drillsite 2.*

A comparison of the transmissivity values for the three groups of PFL fractures in the deformation zones Table 5-1.

Inspection of Figure 5-4 to Figure 5-6 and Table 5-1 do not provide any evidence to suggest that a correlation exits between PFL fractures that are assumed to be critically stressed, because they meet the slip criterion, and PFL fracture transmissivity. This is not surprising as fracture roughness and small scale rock bridges greatly enhance the strength of a fracture, but play less role in the hydraulic transmissivity of a fracture. The lack of seismicity in the region is also an indicator that these fractures at Forsmark are not critically stressed.

Table 5-1. Comparison of the transmissivity values and the dilation (D) and slip (S) potential for PFL fractures in deterministically modelled deformation zones.

	Number	D	S	Log[T] (m^2/s)		
	PFL	Mean	mean	Min	Mean	Max
Gently dipping	120	0.95	3.6	–9.47	–7.16	–2.9
NE-SW steeply dipping	42	0.07	0.37	–9.56	–7.88	–4.7
NW-SE steeply dippning	47	0.08	0.39	–9.35	–7.17	–4.7

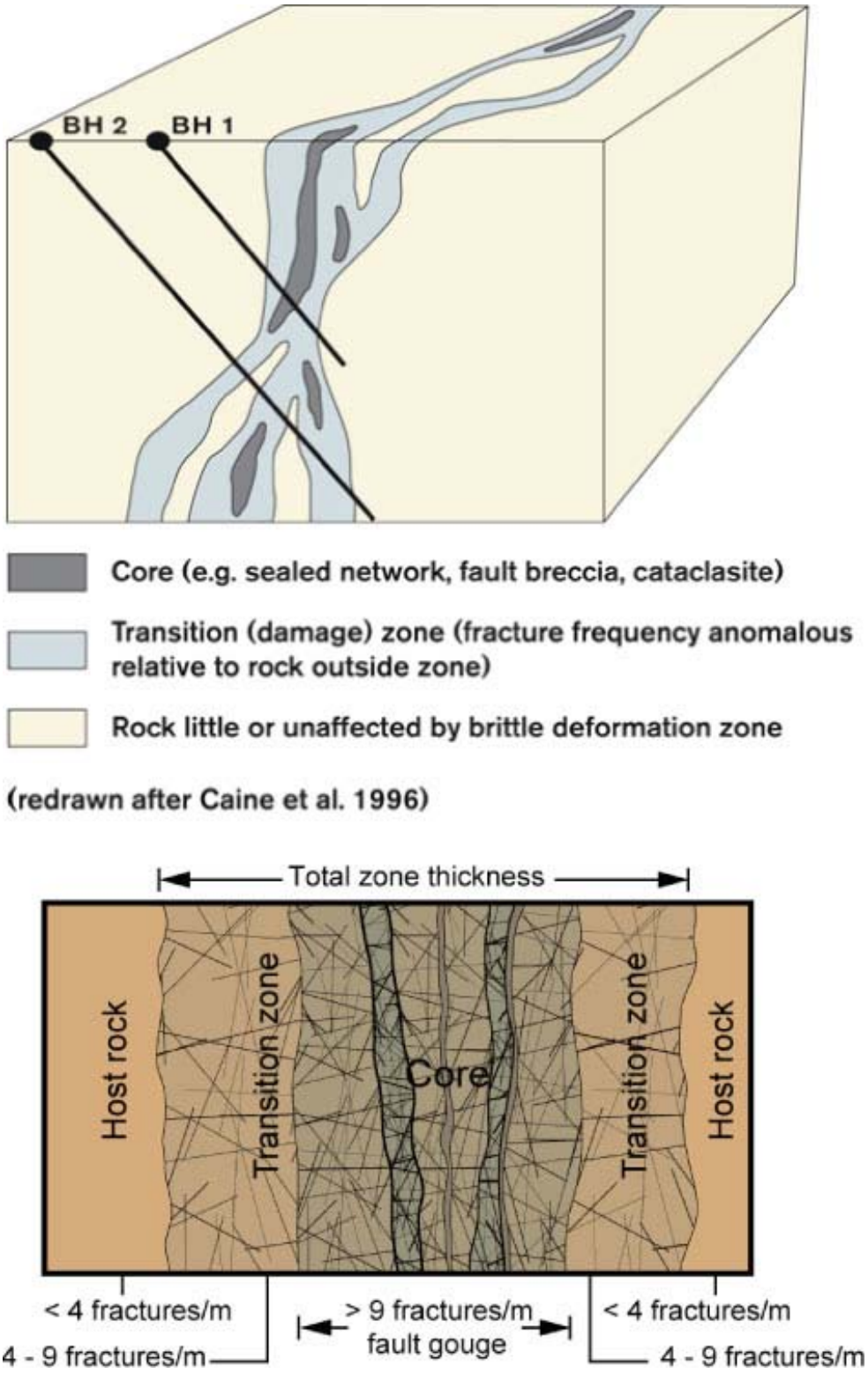

Figure 5-3. *Illustration of the typical fracturing associated with faults. The major deformation zones at Forsmark display various degrees of the fracturing shown in this illustration.*

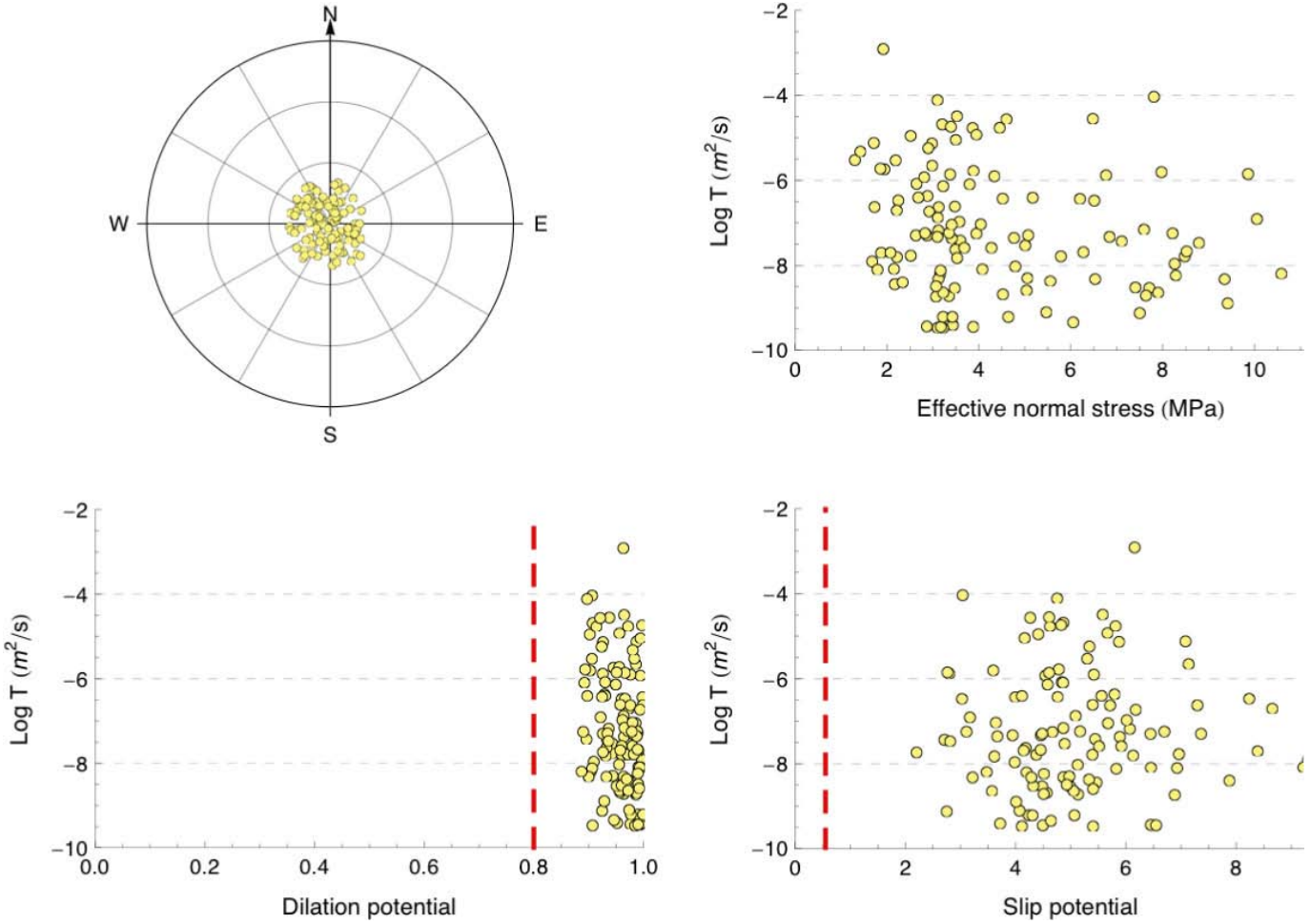

Figure 5-4. *Evaluation of the potential for dilation and slip on 120 gently dipping PFL fractures in deformation zones.*

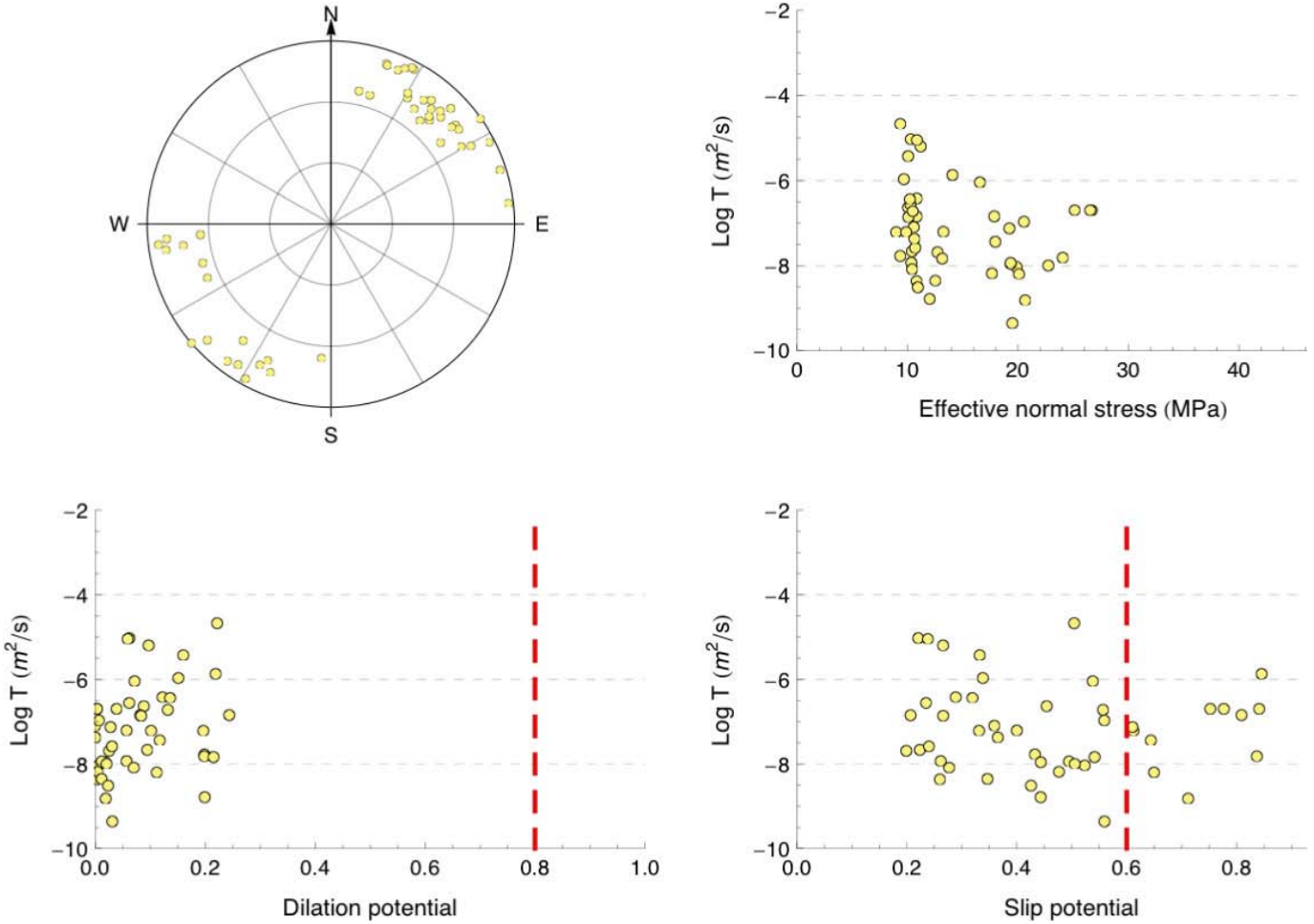

Figure 5-5. *Evaluation of the potential for dilation and slip on 47 NW-SE steeply dipping PFL fractures occurring in deformation zones.*

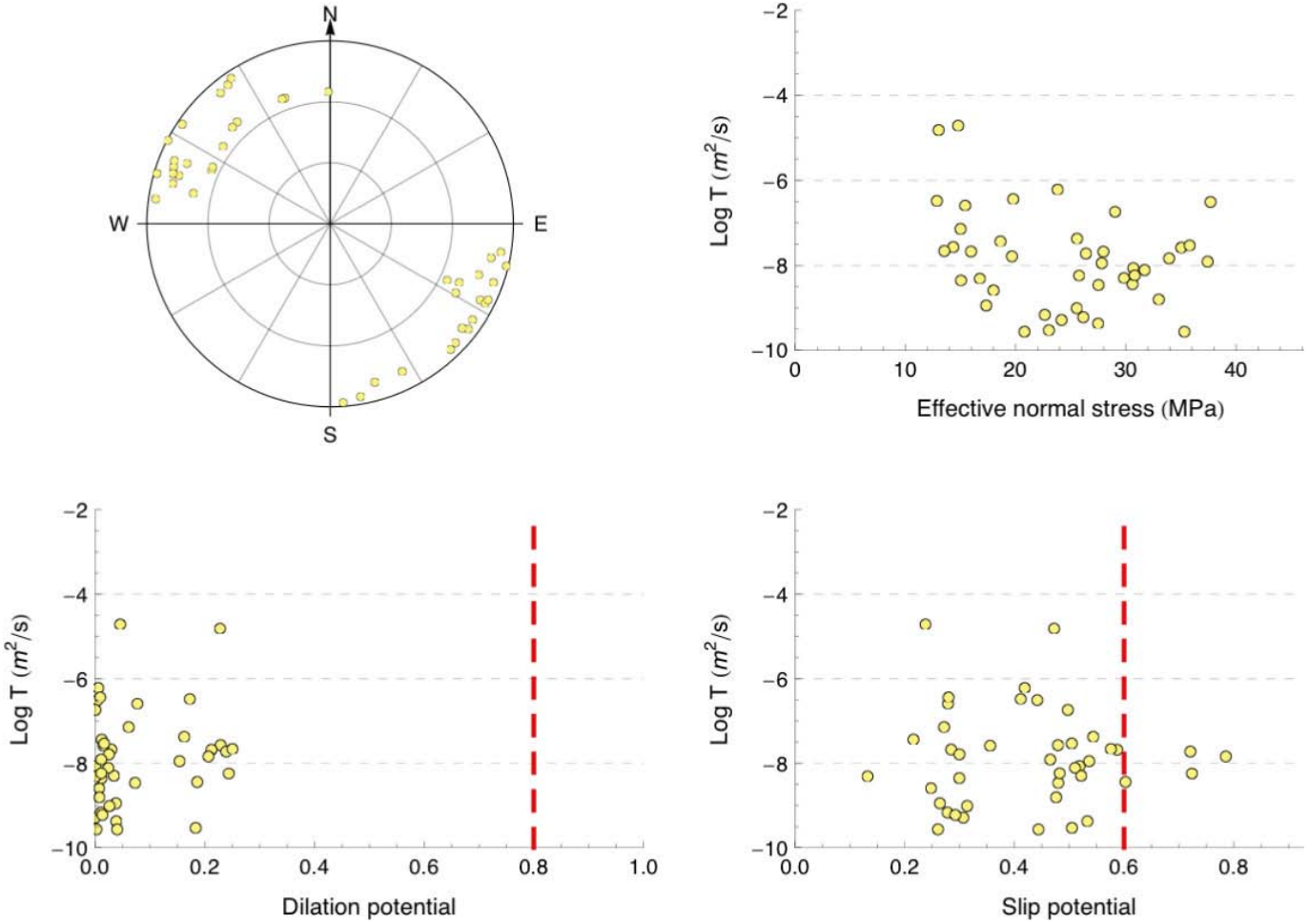

Figure 5-6. *Evaluation of the potential for dilation and slip on 42 NE-SW steeply dipping PFL fractures occurring in deformation zones.*

6 Discussion

The data shown in Chapter 2 (Figure 2-8, Figure 2-10 and Figure 2-11) and the analyses shown in Chapter 4 (Figure 4-2 through Figure 4-11) suggest that there is a reduction in the PFL fracture transmissivity values with depth. Because the stress magnitudes also increase with depth regardless of orientation it may be inferred that the reduction in PFL fracture transmissivity values is related to the increases in stress acting on transmissive fractures. However, as shown in Figure 6-1 the measured frequency of open fractures mapped in the cored boreholes at Forsmark also decreases with depth. This is particularly noticeable in the gently dipping open fractures (compare Figure 6-1 (b) and Figure 4-2). It should also be noted that recording an open fracture in a core log does not imply that the fracture should be classed as a hydraulic feature. For example, Follin et al. (2007a) note that approximately 24% of all fractures mapped in cored boreholes between –100 m and –1,000 m elevation are open but only approximately 7% of the open fractures are detected as flowing with the Posiva Flow Log.

The maximum horizontal stress at Forsmark is trending at approximately 145° and the magnitude of the maximum horizontal stress is approximately twice the minimum horizontal stress. Hence, steeply dipping fractures could be subjected to significantly different normal stresses depending on their orientation. Figure 6-2 compares PFL fracture transmissivity values of steeply dipping PFL fractures for the three categories of hydrogeological data analysed, ALL_PFL, FFM_PFL and ZFM_PFL, see Chapter 3 for details. These data cover normal stress magnitudes ranging from 10 to 40 MPa.

Inspection of Figure 6-2 does not reveal any evidence to suggest there is a correlation between stress and transmissivity for this stress range. However, Figure 6-2 does indicate that the NE-SW steeply dipping PFL fractures consistently have features that display transmissivity values lower than 10^{-9} m^2/s in all three categories. This is particularly noticeable in the ZFM_PFL data set, where a significant number of deformation zones have transmissivity values assigned 10^{-10} m^2/s, i.e. lower than the lower detection limit of the Posiva Flow Log.

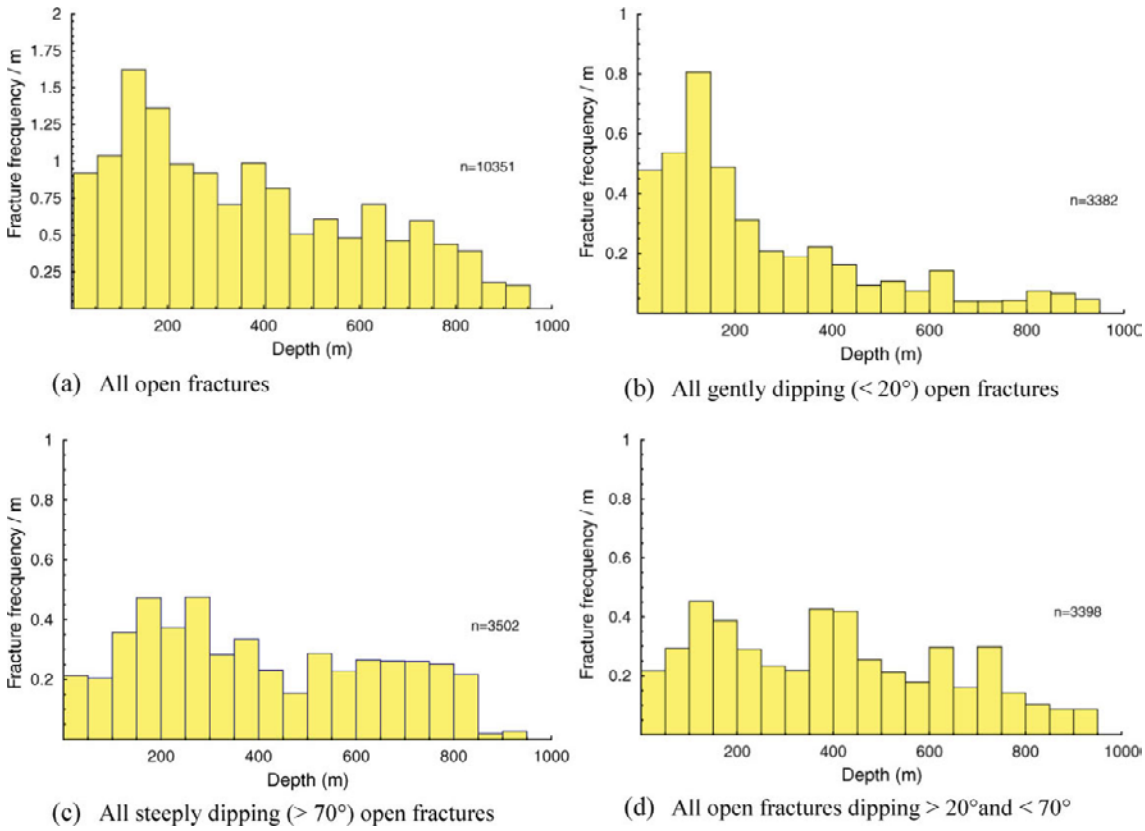

Figure 6-1. *Measured frequencies of Open fractures in cored boreholes at Forsmark visible on the BIPS log.*

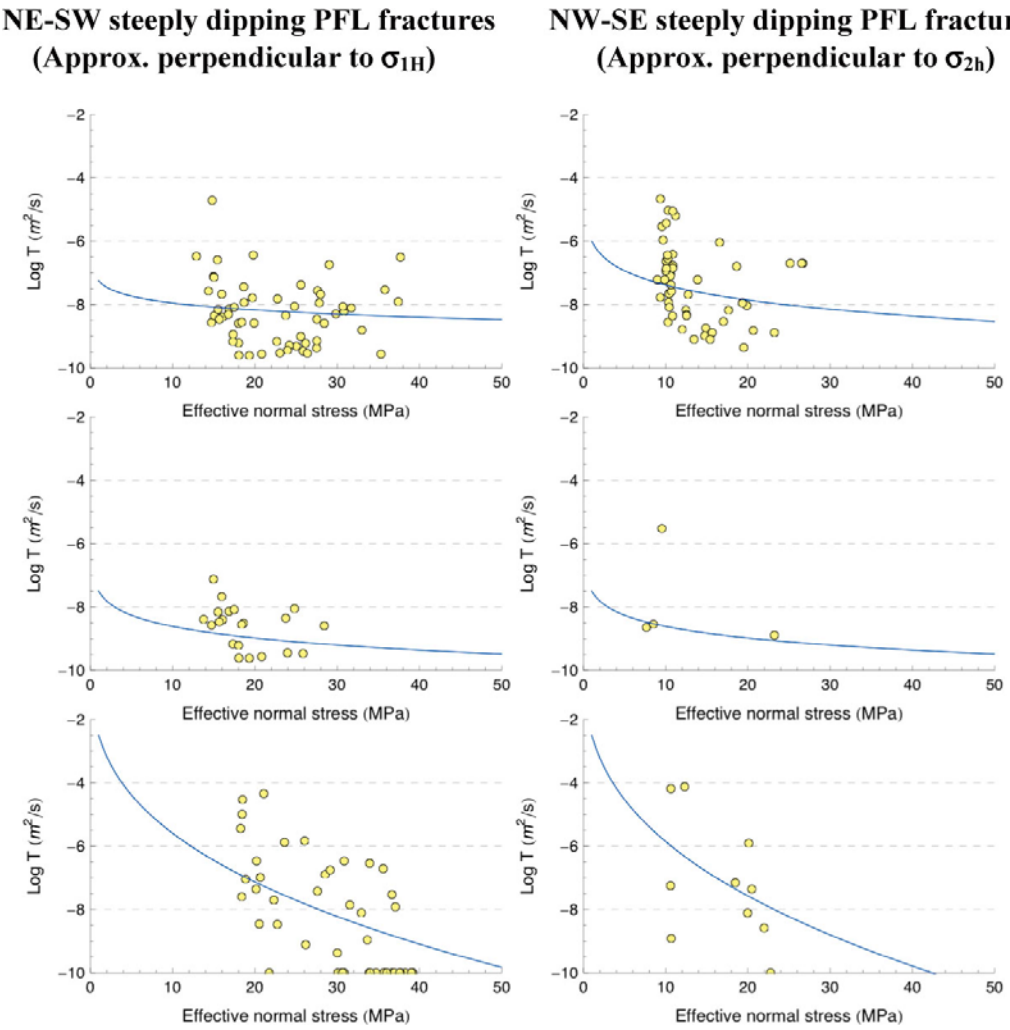

Figure 6-2. *Comparison of normal stress versus the logarithm of PFL fracture transmissivity values of steeply dipping PFL fractures for the three categories of hydrogeological data analysed, ALL_PFL (top row), FFM_PFL (middle row), and ZFM_PFL (bottom row). The solid trend line is based on Equation 1-1.*

According to Indraratna et al. (1999) little or no decrease in transmissivity occurs when the confining stress on laboratory samples exceeds 10 MPa. Hence, because of the 10 to 40 MPa stress range for the steeply dipping PFL fractures, the PFL fracture transmissivity values may not show any relationship to the normal stress. However, the majority of gently dipping fractures are subjected to normal stresses ranging from 1 to 15 MPa. Those results are plotted in Figure 6-3. The results in Figure 6-3 suggest that there may be a relationship between normal stress and PFL fracture transmissivity values. However, Figure 6-1(b) shows that the frequency of gently dipping open fractures in the core logs is drastically reduced with depth, and the apparent trend in Figure 6-3 may be biased by the reduction in the number of gently dipping open fractures with depth. The ZFM_PFL in Figure 6-3 show a noticeable decrease in transmissivity with increasing effective normal stress. The effective normal stress ranges from 1 to 13 MPa, which according to Indraratna et al. (1999) is the range of where the normal stress should have a significant impact.

Figure 6-2 and Figure 6-3 show the trend of Equation (1-1) used to match the trend established from the moving median technique described in Chapter 4. The values for α in Figure 6-2 and Figure 6-3 are compiled in Table 6-1 and compared with laboratory values reported by Olsson (1998) for Äspö diorite and Iwano and Einstein (1995) and Raven and Gale (1985) for igneous crystalline rock.

Note that in Table 6-1 the numbers in the parenthesis for the Gently dipping, NE-SW and NW-SE steeply dipping do not add to the number given for the "All" category because the features that dip between 20° and 60° have not been included in this table except for the ZFM_PFL category.

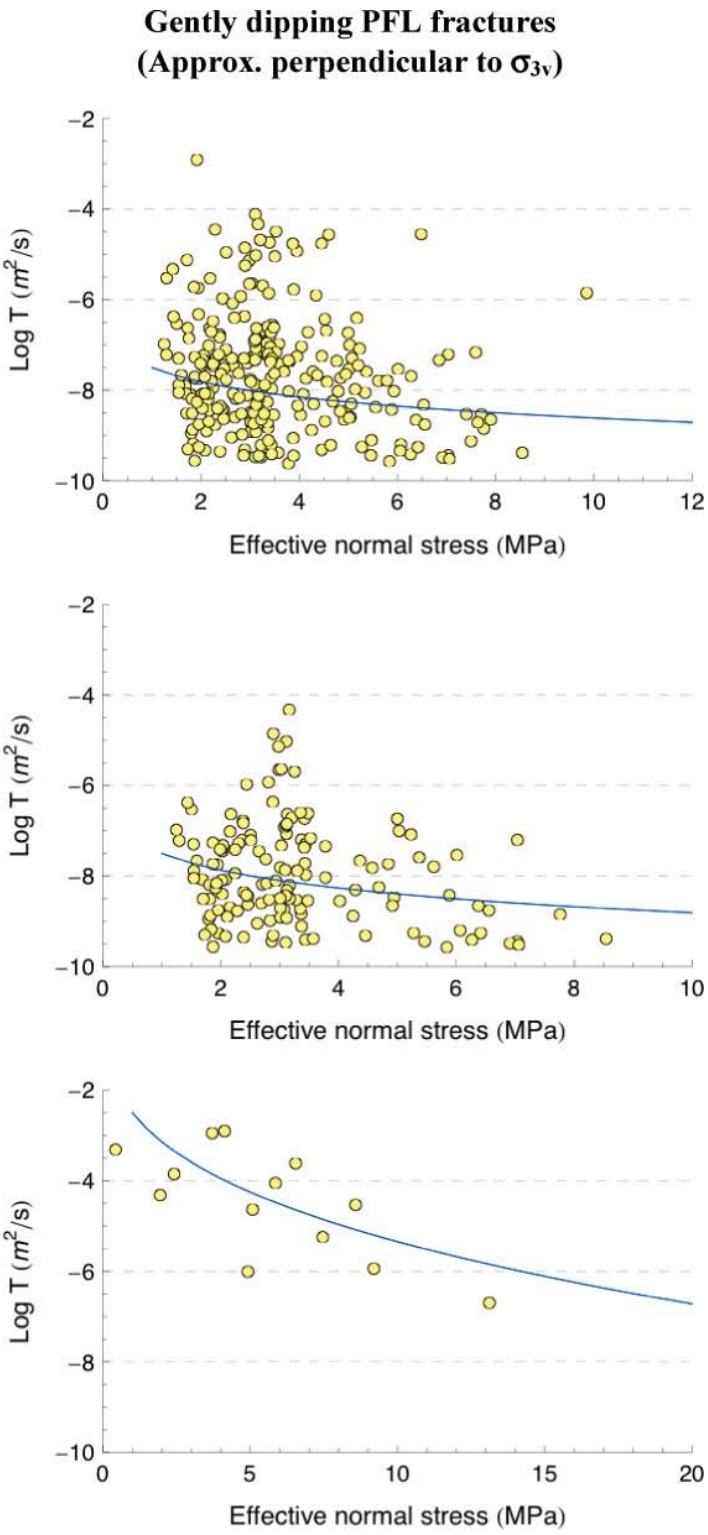

Figure 6-3. *Comparison of normal stress versus the logarithm of PFL fracture transmissivity values of gently dipping PFL fractures for the three categories of hydrogeological data analysed, ALL_PFL (top row), FFM_PFL (middle row), and ZFM_PFL (bottom row). The solid trend line is based on Equation 1-1.*

Table 6-1. Comparison of values of alpha (α) in Equation (1-1) determined from laboratory tests with those determined in the work reported here from the in situ hydrogeological testing programme at Forsmark. The number in the parentheses represents the number of data points used in the analyses.

	Entire Volume	Target Volume		
		ALL_ PFL	FFM_PFL	ZFM_PFL
Field: All	–0.04 (613)	–0.04 (457)	–0.05 (193)	–0.35 (70)
Field:Gently dipping (<20°)	–0.06 (282)	–0.06 (256)	–0.07 (140)	–0.33 (13)
Field:NE-SW steeply dipping	–0.04 (71)	–0.04 (58)	–0.06 (21)	–0.35 (47)
Field:NW-SE steeply dipping	–0.08 (73)	–0.09 (52)	–0.06 (4)	–0.37 (10)
Lab: Olsson 1998	–2.145			
Lab: Iwano and Einstein 1995	–1.344 to –1.703			
Lab: Raven and Gale 1985	–1.09 to –1.89			

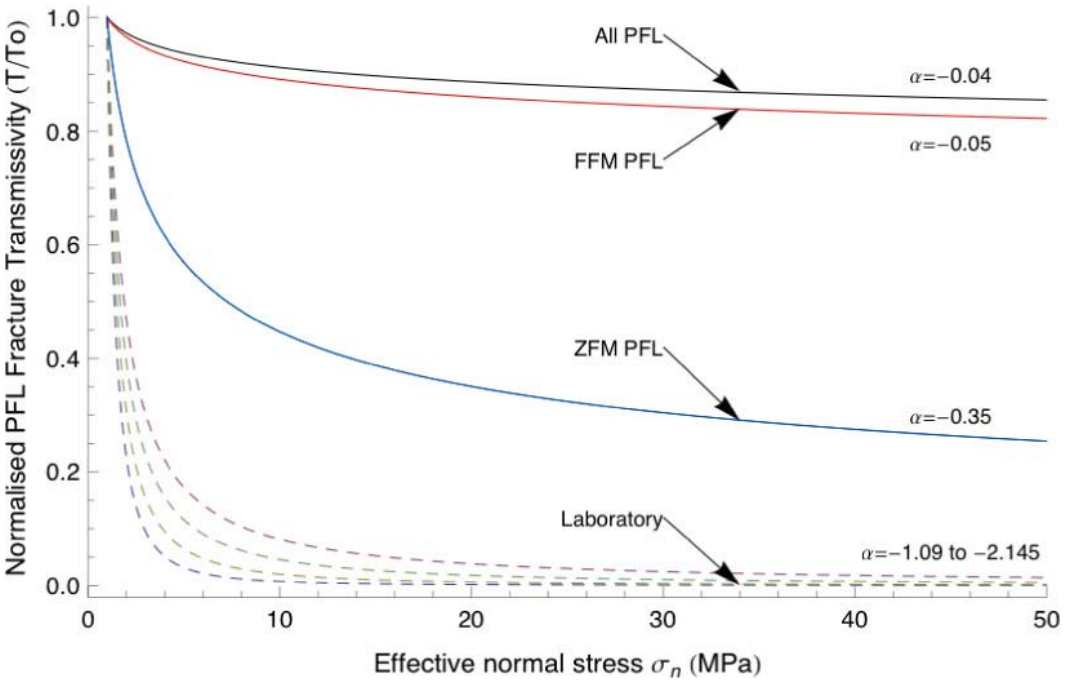

Figure 6-4. *Comparison of the fitted trend lines using Equation 1-1 for the three categories of hydrogeological data analysed, ALL_PFL, FFM_PFL, and ZFM_PFL, and the laboratory value reported by Olsson (1998).*

Figure 6-4 provides a comparison of the values of α for "All" the *in situ* data in Table 6-1 compared with the laboratory value reported by Olsson (1998). The values for T_0 have been normalised so that all the initial values for T_0 are 1. Figure 6-4 shows a significant difference between the stress-flow relationship established from the laboratory behaviour of a single joint (Olsson 1998) and the Forsmark *in situ* data (this study). As noted by Indraratna et al. (1999), Pyrak-Nolte and Morris (2000), and others, the laboratory data suggests there is little impact of the stress on the flow values once the stress acting on the fracture exceeds 10 MPa. Inspection of Table 6-2 shows that none of the α values from the in situ data approach the laboratory values of 2.145. Low α values in laboratory tests tend to indicate smooth fractures, i.e. the smoother the fracture the lower the α value. The PFL fractures studied at Forsmark are of a much larger scale than the laboratory test samples, and it is unlikely that the lower α values measured for the *in situ* data implies smooth fractures. There does not appear to be sufficient evidence to support the notion that the normal stress acting on the fracture solely controls the magnitude of the flow along the fractures at Forsmark.

7 Conclusions

The hydrogeological data for Forsmark consists of hydraulic data of discrete fractures and integrated transmissivity data associated with deterministically modelled deformation zones. For both sets of features, geological information is provided.

First, the work reported here assumes that the specific capacity values measured with the PFL method and reported to Sicada as PFL fracture transmissivity data represent the local transmissivity values at the borehole, i.e. the transmissivity of the intersecting flowing fractures.

Second, it is assumed that the correlation analyses carried out by Forssman et al. (2004, 2008) and Teurneau et al. (2008) give the correct fracture orientations.

Third, the analysis of PFL for stress analysis is divided into three hydrogeological categories:

1. **ALL_PFL**: This data set is used to assess the general trend in all PFL data, i.e. both inside and outside the target volume regardless of spatial location or geological context. It consists of 613 PFL data.
2. **FFM_PFL**: This data set is used to assess the trend in the PFL inside the target volume, i.e. data spatially distributed within fracture domains FFM01, FFM02, and FFM06. It consists of 271 PFL data.
3. **ZFM_PFL**: This data set is used to asses the trend in 70 deterministically modelled deformation zones that occur inside or in close proximity to the target volume. Transmissivity values of deterministically modelled deformation zones are obtained by adding all individual values between the defined geometrical bounds of each deformation zone. Deformation zones with little or no flow have been assigned an arbitrary low transmissivity value of 1×10^{-10} m^2/s, see Figure 2-8. The 70 deformation zones have been assigned the following orientation categories: G (gently dipping; 13), ENE (36), NE (3), NNE (8), NNW (3), NW (3), and WNW (4).

In the present work, systematic analyses are carried out to explore possible relationships between the PFL fracture transmissivity data and the normal stress acting on each PFL fracture. The main findings from these analyses are:

1. No relationship is found between PFL fracture transmissivity and normal stress for the steeply dipping fractures. The normal stress ranged from 10 to 40 MPa. Indraratna et al. (1999) note that when the confining stress on laboratory samples exceeds 10 MPa, little or no decrease in transmissivity occurs.
2. There is some evidence that the PFL fracture transmissivity of the gently dipping fractures decreases with depth. However, because both the frequency of gently dipping open fractures decreases with depth and the normal stress is also increasing with depth it is not possible to sort out cause and effect for these gently dipping PFL fractures. The gently dipping ZFM_PFL show the strongest correlation between stress and transmissivity. For these zones the effective normal stress is in the range of 1 to 13 MPa.
3. Comparison of the value for α for the empirical Equation 1-1 that links stress and transmissivity shows that there is little or no agreement between the *in situ* values for α (–0.04 to –0.28) and the laboratory values (–1 to –2.15).
4. Comparison of the dilation and slip potential of the fractures and the measured transmissivity values shows there is no increase in transmissivity as the slip and dilation potential increases or decreases.

In conclusion, there does not appear to be sufficient evidence from these analyses to support the notion that the magnitude of the flow along the fractures at Forsmark is solely controlled by the normal stress acting on the fracture. This should not be surprising because the majority of the fractures formed more than 1 billion years ago and the current stress state has only been active for the past 12 million years. It is more likely that the transmissivity values are controlled by fracture roughness, open channels within the fracture and fracture infilling material. The role of mineral infilling and its effect on fracture transmissivity should be explored further.

8 References

SKB's (Svensk Kärnbränslehantering AB) publications can be found at www.skb.se/publications.

Andersson J, Ström A, Svemar C, Almén K-E, Ericsson LO, 2000. Vilka krav ställer djupförvaret på berget? Geovetenskapliga lämplighetsindikationer och kriterier för lokalisering och platsutvärdering. SKB R-00-15, Svensk Kärnbränslehantering AB. (In Swedish.)

Barton C A, Zoback M D, Moos D, 1995. Fluid flow along potentially active faults in crystalline rock. Geology, 23, pp 683–686.

Byerlee J D, 1978. Friction of rocks. Pure and Applied Geophysics, 116, pp 615–626.

Cloos E, 1955. Experimental analysis of fracture patterns. Geological Society of America Bulletin, 66, pp 241–256.

Esaki T, Nakahara K, Jiang Y, Kimura T, Mitani Y, 1995. Shear-flow coupling properties of rock joints. In: Fujii T (ed). Proceedings of the 8th ISRM Congress on Rock Mechanics, Tokyo, 25–29 September 1995. Vol 3. Rotterdam: Balkema, pp 739–742.

Ferrill D A, Winterle J, Wittmeyer G, Sims D, Colton S, Armstrong A, Morris A, 1999. Stressed rock strains groundwater at Yucca Mountain, Nevada. GSA Today, 9, pp 1–8.

Follin S, 2008. Bedrock hydrogeology Forsmark. Site descriptive modelling, SDM-Site Forsmark. SKB R-08-95, Svensk Kärnbränslehantering AB.

Follin S, Levén J, Hartley L, Jackson P, Joyce S, Roberts D, Swift B, 2007a. Hydrogeological characterisation and modelling of deformation zones and fracture domains, Forsmark modelling stage 2.2. SKB R-07-48, Svensk Kärnbränslehantering AB.

Follin S, Johansson P-O, Hartley L, Jackson P, Roberts D, Marsic N, 2007b. Hydrogeological conceptual model development and numerical modelling using CONNECTFLOW, Forsmark modelling stage 2.2. SKB R-07-49, Svensk Kärnbränslehantering AB.

Follin S, Hartley L, Jackson P, Roberts D, Marsic N, 2008. Hydrogeological conceptual model development and numerical modelling using CONNECTFLOW, Forsmark modelling stage 2.3. SKB R-08-23, Svensk Kärnbränslehantering AB.

Follin S, Ludvigson J-E, Levén J, 2011. A comparison between standard well test evaluation methods used in SKB's site investigations and the generalised radial flow concept. SKB P-06-54, Svensk Kärnbränslehantering AB.

Forssman I, Zetterlund M, Rhén I, 2004. Correlation of Posiva Flow Log anomalies to core mapped features in Forsmark (KFM01A to KFM05A). SKB R-04-77, Svensk Kärnbränslehantering AB.

Forssman I, Forsmark T, Rhén I, 2008. Forsmark site investigation. Correlation of Posiva Flow Log anomalies to core mapped features in KFM02B, KFM 08D and KFM 11A. SKB P-07-128, Svensk Kärnbränslehantering AB.

Glamheden R, Fredriksson A, Röshoff K, Karlsson J, Hakami H, Hakami E, Christiansson R, 2007. Rock Mechanics Forsmark. Site descriptive modelling, Forsmark stage 2.2. SKB R-07-31, Svensk Kärnbränslehantering AB.

Indraratna B, Ranjith P G, Gale W, 1999. Single phase water flow through rock fractures. Geotechnical and Geological Engineering, 17, pp 211–240.

Iwano M, Einstein H H, 1995. Laboratory experiments on geometric and hydromechanical characteristics of three different fractures in granodiorite. In: Fujii T (ed). Proceedings of the 8th ISRM Congress on Rock Mechanics, Tokyo, 25–29 September 1995. Vol 2. Rotterdam: Balkema, pp 743–750.

Olofsson I, Simeonov A, Stephens M, Follin S, Nilsson A-C, Röshoff K, Lindberg U, Lanaro F, Fredriksson A, Persson L, 2007. Site descriptive modelling Forsmark, stage 2.2. A fracture domain concept as a basis for the statistical modelling of fractures and minor deformation zones, and interdisciplinary coordination. SKB R-07-15, Svensk Kärnbränslehantering AB.

Olsson R, 1998. Mechanical and hydromechanical behaviour of hard rock joints: a laboratory study. PhD thesis. Department of Geotechnical Engineering, Chalmers University of Technology, Göteborg, Sweden.

Pyrak-Nolte L J, Morris J P, 2000. Single fractures under normal stress: the relation between fracture specific stiffness and fluid flow. International Journal of Rock Mechanics and Mining Sciences, 37, pp 245–262.

Raven K G, Gale J E, 1985. Water flow in a natural rock fracture as a function of stress and sample size. International Journal of Rock Mechanics and Mining Sciences & Geomechanics Abstracts, 22, pp 251–261.

Rogers S F, 2003. Critical stress-related permeability in fractured rocks. In: Ameen M (ed). Fracture and in situ stress characterization of hydrocarbon reservoirs. London: Geological Society. (Geological Society Special Publication 209), pp 7–16.

Rouhiainen P, Sokolnicki M, 2005. Forsmark site investigation. Difference flow logging in borehole KFM06A. SKB P-05-15, Svensk Kärnbränslehantering AB.

Skempton A W, 1966. Some observations on tectonic shear zones. In: Proceedings of the 1st Congress of the International Society for Rock Mechanics, Lisbon, 25 September – 1 october 1966. Vol 1. International Society for Rock Mechanics, pp 329–335.

Stephens M B, Fox A, La Pointe P, Simeonov A, Isaksson H, Hermanson J, Öhman J, 2007. Geology Forsmark. Site descriptive modelling Forsmark stage 2.2. SKB R-07-45, Svensk Kärnbränslehantering AB.

Thiem G, 1906. Hydrologische Methoden. Leipzig: Gebhardt.

Teurneau B, Forsmark T, Forssman I, Rhén I, Zinn E, 2008. Forsmark site investigation. Correlation of Posiva Flow Log anomalies to core mapped features in KFM01D, KFM07C, KFM08A, KFM08C and KFM10A. SKB P-07-127, Svensk Kärnbränslehantering AB.